A Method to Design Hybrid Lattice Support Structures for LPBF Additive Manufacturing

submitted in partial fulfillment of the requirements for

the degree of

Doctor of Philosophy

in

Department of Mechanical Engineering

Lisha White

B.S., Engineering, James Madison University
M.S., Mechanical Engineering, Carnegie Mellon University

Carnegie Mellon University
Pittsburgh, PA

December 2023

Acknowledgments

I would like to thank my doctoral committee, Professor Jonathan Cagan, Professor Yongjie Jessica Zhang, Professor Anthony Rollett, and Dr. Guanglu Zhang, for their support and advice on this dissertation.

This research was partially sponsored by the Army Research Laboratory under Cooperative Agreement Number W911NF-18-2-0162. The views and conclusions contained in this document are those of the authors and should not be interpreted as representing the official policies, either expressed or implied, of the Army Research Laboratory or the U.S. Government. The U.S. Government is authorized to reproduce and distribute reprints for Government purposes notwithstanding any copyright notation herein. L. White is also partially supported by The National GEM Consortium Fellowship.

Abstract

Support structure design is imperative in the design of additively manufactured parts with overhang features in the build direction, especially those fabricated using laser powder bed fusion (LPBF). When designed effectively, support structures quickly dissipate heat and mitigate part distortion without driving up excessive costs. Lattices, composed of individual unit cells strategically arranged to achieve a desired function, are a promising solution as a support structure (e.g., tunable properties, reduction in manufacturing costs). Despite their potential, two main drawbacks are (1) the computational cost to find an optimally directed solution and (2) the adaptability to complex support structures. Prior research has designed lattice support structures utilizing both gradient- and non-gradient-based optimizers; however, there still exist limitations within the current work. Gradient-based optimizers pose challenges regarding limited design exploration and non-differentiable objective function. Non-gradient-based optimizers, proven to be an effective alternative solution, are known to be too slow in comparison to gradient-based optimizers and have not yet been applied to consider the multi-physics functionality of support structure. Furthermore, the box-like structure of the unit cells makes it difficult to apply to complex structures. Current methods employing non-solid and solid pin supports are unreliable for curved or inclined surfaces. Thus, to improve the current state of the design of support structures, a robust method to facilitate the design of lattice support structures and a multi-sized unit cell approach using LPBF is proposed.

The proposed method addresses the two defined roadblocks of computational cost and adaptability and provides validation for each through three works. The first two works address the high computational cost associated with significant design exploration and using simulation-informed evaluations are addressed by modifying a non-gradient based optimizer, simulated annealing (SA). The modified SA-based method is utilized to quickly optimize the distribution of commonly employed, pre-defined unit cells while adhering to user-defined manufacturing constraints. By incorporating a stage-dependent annealing swapping strategy, a decrease in iteration count to explore the domain is achieved for multiple scales. Combined approximation techniques of homogenization and equivalent static loading reduce the computational cost of simulation-informed evaluations. Furthermore, a multi-sized unit cell approach is proposed to enable

lattice support structure design for complex geometries, addressed in the last work. The problem is formulated to find the optimal configuration to dissipate heat while considering structural integrity and manufacturing costs (e.g., material and post-processing costs). The method is validated through several case studies, including a cantilever beam, aerospace bracket, and heat exchanger adapter. Within each case study, consistently obtained increased heat dissipation is accomplished and compared to the uniformly distributed benchmark design while still satisfying manufacturing constraints. For the case study of a cantilever beam and aerospace bracket, up to 61% reduced material cost and 62% reduced post-processing costs are achieved, while satisfying constraints. For the intricate design of the heat exchanger adapter, at least 50% of material cost savings are achieved which is about 19% of the total cost of the entire build. Overall, this dissertation seeks to help users design complex LBPF geometries with customizable support structure properties. It will also advance the current research within a range of disciplines, including design, optimization, and AM of lattices.

Table of Contents

List of Tables

List of Figures

1. Chapter 1: Introduction

1.1. Motivation

Additive manufacturing (AM) is a rapidly expanding industrial field due to its ability to create customizable, complex structures [1]. Laser Powder Bed Fusion (LPBF) is a popular approach in the creation of metal parts within AM. This approach has been repeatedly proven to create structures such as topology-optimized structures for reduced weight and components with internal channels. To create such intricate features, a concentrated, high-energy heat source fuses metal powder layers to solid metal layers in the desired cross-section [1,2]. After each layer is spread, melted, and solidified, another layer of powder is added, and the process is repeated until the final part is created. Although this process has many advantages compared to traditional manufacturing techniques (e.g., milling and casting), challenges still exist that need to be considered when designing a part. One challenge is due to the rapid heating of the solid powder and cooling of the liquid metal, which limits the types of metals that are suitable for this process [1]. Within that selection, the quality of the part is dependent on many factors such as part orientation [3], printing parameters [4–6], and support structure design [7,8]. Another challenge is regarding the cost to manufacture, mainly attributed to the cost of the powder material [1,9]. Therefore, designers must make informed decisions to justify the fabrication of a part using LPBF that drives down the cost to design and manufacture.

Support structures are a necessary expense when designing parts with overhang features. These downward-facing surfaces are typically greater than 5 mm in length and oriented less than 45° with respect to the base plate [10,11]. In part due to the low thermal conductivity of the surrounding powder and rapid thermal cycle, support structures serve two main functions for overhangs: to transfer heat and to anchor the part to the base plate [10–13]. Poor design of these structures will lead to part inaccuracy and may damage the machine, both factors which will significantly increase the cost to manufacture. Therefore, optimization techniques play a critical role in the design of these support structures for functionality, printability, and

cost reduction [14]. In addressing those three pillars, lattice design optimization is a promising solution [10,15–17]. A lattice is composed of self-supporting unit cells that are strategically designed on a microscopic scale and distributed within the design domain to achieve specific macroscopic properties. Researchers have introduced optimization methods to generate lattice support structures by using combinations of the unit cells [1,2,10,11]. Despite its promise, lattice support structures have not been widely applied as support structures. This may be attributed to two main drawbacks: (1) the computational cost to generate an optimally directed solution and (2) the attachment of lattice support structures to complex structures.

Within support structure design, the lattice support structures are typically computationally designed with the main objective to either dissipate heat or minimize compliance of the part. Optimization methods previously proposed typically frame the problem in a continuous domain by either redistributing material in the design domain or of a unit cell that is periodically repeated using gradient-based optimization techniques [13,15,16,18]. In doing so, challenges regarding non-differentiable design variables and limited design exploration emerge. Non-gradient-based optimization is an alternative solution [19,20] but the approach is relatively slow compared to gradient-based optimizers due to the computational cost required to search the design domain. In summary, existing non-gradient and gradient-based optimization methods require high computational costs to find a 'good' solution. Of the two techniques, non-gradient-based optimizers are the most promising technique due to their inherently high design exploration characteristic. Therefore, one research question to address is: how can designers *efficiently* find an optimally directed lattice support structure solution that improves heat dissipation while satisfying multiple AM constraints for LPBF?

Another shortcoming preventing adaptation of lattice support structure for LPBF is the connection between the lattice and the part [17,21,22]. It is imperative for designers to consider the transitioning area as it is prone to generate cracks at the interface of the solid and lattice support [17,21–24]. Generally, a unit cell has a box-like shape which is ideal for fitting to horizontal overhangs, such as a cantilever beam.

However, one of the main advantages of LPBF is its ability to create complex components that would be unattainable through subtractive metal manufacturing procedures (e.g. laser cutting). Thus, limiting the optimization of lattice support structures to horizontal design domains restricts their practical use within industrial applications. Few researchers have addressed this problem by designing various connectors between the part and the lattice structure [7,17,21–23,25]. For connecting to non-horizontal surfaces, a popular approach is to employ either non-solid (e.g., point or thin-wall) [7,23,25–27] or solid pin [7,21,26] connections to reduce the cost associated with the material and post-processing. Utilizing non-solid connections, such as block structures, have low contact area and have been known to fail during printing for parts with large residual stresses [16,22,26,27]; thus, pin connections are seen as an alternative [26]. Pin connections can enable larger contact between the part and lattice support structure but the distancing and size of contact need to also be computationally designed [28]. By parameterizing both pins and lattice, there will exist high computational costs to explore the design domain with a significant number of design variables [19,21]. Additionally, optimizers must also be able to evaluate the configurations every iteration. Evaluating the properties of the non-uniform distribution of non-solid or solid pin connections also increases the computational cost between iterations [17,23]. Solid connections are a simple solution that could be included to create the desired horizontal surface but will result in increased material cost when utilizing single-unit cell sizes. Therefore, another research question arises: how can lattice support structures be computationally designed to be *attached* to complex structures?

To address these questions for support structure design, we propose a method to utilize a modified, non-gradient-based optimizer to generate support structures that adhere to multiple AM constraints without excessive computational time. This goal is achieved within a three-part procedure. We will (1) introduce a method to design lattice support structures for heat dissipation with reduced computational cost per run and iteration; (2) modify the proposed method to design optimally directed lattice support structures that consider both the thermal and structural functionality; and (3) develop an approach to design lattice support structures for complex geometries. This research will provide the necessary process for advancing the

current state-of-the-art methods to manufacture lattice and support structures for LPBF and other AM techniques.

1.2. Thesis Statement

Based on the research gaps presented in Section 1.1, two aims are defined for this dissertation with the overarching goal to reduce design and manufacturing costs for designers. The first aim of this work is to increase the efficiency of non-gradient-based optimizers for AM applications through the design of support structures. Accordingly, the new design opportunity of utilizing a non-gradient-based optimizer, simulated annealing (SA), to generate thermally conductive lattice support structures for LPBF with reduced computational cost is investigated. By modifying the traditional SA optimizer, a method is proposed to find an optimally directed solution to maximize the dissipation of heat while considering practical AM constraints such as structural integrity, material waste, and post-processing. This method broadens the capabilities of non-gradient-based optimizers by introducing a stage-dependent annealing swapping strategy for efficient design domain exploration. Furthermore, homogenization approximation and equivalent static loading are incorporated for fast iteration evaluation of simulation-informed objectives and constraints.

The second aim of this work is to expand the application of lattice support structures as viable support structures for all AM geometries. To this end, a multi-sized unit approach is established to design lattice support structures for complex geometries containing curved and inclined overhangs. Based on voxel-mesh representation, an automated support design domain is generated—enabling the employment of multi-sized unit cells to reduce material waste. The approach is coupled with the modified SA-based optimization method to create lattice support structures designed for LPBF.

This work aims to support the following thesis:

To reduce manufacturing and design costs of support structures in laser powder-bed fusion, lattice support structures can be computationally designed to maximize the dissipation of heat while constraining

residual stress and deformation for complex structures. By utilizing a modified simulated annealing-based method, designers can efficiently generate optimally directed configurations of pre-defined unit cells with specified functionality at reduced computational costs.

1.3. Dissertation Outline

The remainder of this work is organized to describe the two of the objectives outlined in Section 1.2.

To address the investigation of non-gradient-based optimizers as a viable tool for support structure design, a novel method is introduced and computationally validated. Beginning with **Chapter 2**, a modified-simulated annealing method is presented for the generation of thermally conductive lattice support structures constrained by manufacturing costs. Two approximation techniques, homogenization approximation and equivalent static loading, are employed to reduce the computational cost between iterations. Moreover, a novel stage-dependent annealing swapping strategy is introduced for efficient design exploration.

Further examination of the employment of non-gradient-based optimizers is performed in **Chapter 3** as the multi-functionality of support structures is considered. Both thermal and structural properties of the support structure are evaluated to demonstrate the versatility of previously proposed approximation techniques. A comparative study is also performed to affirm the efficiency of the stage-dependent annealing swapping strategy.

In **Chapter 4**, the challenge of lattice support structure compatibility with complex geometries is addressed. A voxelization approach is introduced to enable the use of multi-sized unit cell supports for reduced material costs. Coupled with the modified-simulated annealing method, the automated identification of multi-sized unit cells enables the design of hybrid lattice support structures for complex LPBF geometries containing curved and inclined overhangs.

The overarching goal of this work is to provide a method to enable designers to minimize manufacturing and design costs of AM structures through the investigation of lattice support structure design. Therefore,

Chapter 5 summarizes the method and results from the preceding three chapters and highlights the major contributions that aid in the foundational solution of employing lattice support structures. In addition, insights are drawn about the potential areas of future work to present limitations and fields of advancement.

2. Chapter 2: A Modified Simulated Annealing-Based Method to Design Thermally Conductive Hybrid Lattice Support Structures for LPBF[1]

2.1. Overview

In this work, a modified simulated annealing-based method is introduced to investigate the design opportunity of utilizing non-gradient-based optimization to maximize heat dissipation while adhering to design for AM cost constraints. The preliminary method facilitates the design of lattice support structures by modifying the traditional simulated annealer (SA) to distribute three commonly employed unit cells to dissipate heat while adhering to user-defined manufacturing cost constraints. By incorporating both stage-dependent annealing swapping strategy, homogenization approximation, and equivalent static loading, multiple solutions are consistently found for the cantilever beam case study. The optimally directed solutions have an average objective function of about 16% better heat dissipation than the uniformly distributed benchmark design with manufacturing constraints satisfied. Further validation is performed with a transient thermal simulation to obtain the time to reach steady-state temperature.

2.2. Introduction

Within laser powder bed fusion (LPBF), a concentrated, high-energy heat source fuses metal powder layers with solid metal layers in the desired cross-section. Ideally, as the heat source translates to create the layer, the liquid metal in its path and a few layers beneath are quickly melted and cooled [1,2,26,30,31]. This can only occur if the heat is able to dissipate from the melted layers to a cooler region, such as the base plate. The low thermal conductivity of the powder and the non-uniform heat distribution, caused by the

[1] L. White, X. Liang, G. Zhang, J. Cagan, Y. J. Zhang. Coupling Simulated Annealing and Homogenization to Design Thermally Conductive Hybrid Lattice Support Structures for LPBF. ASME International Design Engineering Technical Conference & Computers and Information in Engineering Conference (IDETC/CIE). Boston, MA. Aug 20-23, 2023. [29]

small diameter of the high-energy source, causes heat to accumulate in locations not directly connected to the build plate [9,10]. The non-uniform distribution will result in distortions [16,18,31–33], discoloration [26], high surface roughness in the final part [2,34,35], and could damage the machine due to collision between the part and the powder recoater [2]. These deformities are most apparent in parts with downward-facing surfaces that are parallel to the base plate and greater than 5 mm [10,11] in length. In such cases, the support structure is required to both anchor the part to the build plate and to help dissipate heat [10–13].

Due to the capabilities of AM, lattices are a feasible solution for the fabrication of support structures [10,11,32,33]. Lattices are composed of individual unit cells that can be either periodically or non-periodically distributed. These structures are promising because they reduce material waste, possess tailorable mechanical and thermal properties, are self-supporting, and are suitable for powder removal. Thus, extensive research has been conducted to optimize discrete unit cell designs. Specifically for thermal applications, these optimization efforts are typically approached using gradient-based optimizers [36] as they are regarded as more time-efficient than non-gradient-based optimizers. Typical objective functions employed are the minimization of thermal potential energy [37,38], thermal compliance [13,39], average temperature [30], and thermal gradient [18]. Using one or more of these objective functions to find the optimally directed support structure, some optimizer methods find solutions through the use of material elements within the units [13]. This approach leads to large amounts of computational effort due to the highly iterative procedure when optimizing. The high computational effort is evident when numerical methods are required to solve the governing physics equations to obtain simulation-informed support structure designs. In addition, the computation drastically increases with an increasing number of design variables to represent the potential distribution of materials and filtering of the continuous components to have physical meaning.

As an alternative, libraries have been established to allow designers to map printable lattice structures to physical locations. Given the variability of the manufacturability of unit cells [1,40], each library needs to be customized according to the printing parameters, materials, and design requirements for distinct unit

cells. Utilizing topology optimization with gradient-based optimizers for distinct design variables can be challenging [41,42], especially with the added complexity of the sensitivity equations and initial design dependency [32,37]. An alternative approach is the use of non-gradient-based topology optimizers to design lattice support structures for heat dissipation. However, expensive computation has been one bottleneck preventing their application to the design of lattice support structures.

Based on the limitations of existing optimization techniques for lattice support structure designs, a method that improves the efficiency of an existing non-gradient-based optimizer, simulated annealing (SA), is proposed. Modifications to the traditional SA optimizer method have been made to address the computational bottleneck and search the design domain efficiently. Specifically, homogenization approximation and equivalent static loading are integrated into the method to quickly evaluate the steady-state thermal equation. A stage-dependent annealing strategy is created and incorporated into the modified SA method to derive the optimal distribution of unit cells that maximizes heat dissipation while adhering to user-defined manufacturing constraints, such as manufacturing costs.

The remainder of this chapter is organized as follows: In Section 2.3, related work of support structure design and limitations of both gradient and non-gradient-based optimizers are presented. Section 2.4 introduces the governing physics equations, problem statement, and modified simulated annealing-based method for expedited evaluation that will be utilized in this study. Next, Section 2.5 presents the results of the case studies and Section 2.6 draws the conclusion and points out future work.

2.3. Background and related work

The generation of support structures, gradient-based optimization has been utilized to design support structures for heat dissipation whereas non-gradient-based optimization has primarily focused on the application of lattice support structures for structural stability of the part. Several gradient-based optimizer methods have been proposed in prior research to produce promising results but there exist drawbacks such as computational expense or potential suboptimal designs. For example, a gradient-based optimizer method

was employed to generate lattice support structures by minimizing thermal compliance within the system. Although the approach was able to reduce warpage as compared to traditional support structures, such as pillars, it optimized one unit cell that was repeated periodically. This method may lead to excessive amounts of material in some areas, particularly with the non-uniform distribution of heat applied at the top layer that does not result in uniform cooling. To capture both the non-uniformity and the time-dependency of heat dissipation, recent work has considered the transient temperature effects for the dissipation of heat and the mechanical properties [18]. Evaluation of the macroscale lattice is accelerated by coupling a library composed of the relative densities of a simple cubic structure's effective properties with the HA, which employs RVEs [16,18,37,43]. This drastically reduces the number of design variables from microscale material elements to mesoscale unit cells to choose for each possible location [16,18,37,44]. By utilizing a gradient-based optimization method, the model was able to reduce the liquid lifetime (i.e., the amount of time the top layer is above liquid temperature) and reduce the residual deformation by 42% when compared to the benchmark of a uniformly sized simple cubic lattice support structure. However, only a simple cubic unit cell was optimized for the density, limiting the method's ability to consider more AM constraints, such as reducing contact area for reducing post-processing costs [1,35,45,46].

As an alternative, non-gradient-based optimizers, such as simulated annealing (SA) and genetic algorithms (GA), are reputable for optimizing problems with discrete design variables [41,42]. Both SA and GAs use a stochastic optimization approach that allows for a broader search of the design domain, overcoming potential local optima. GA is based on Darwinian evolution to find one or multiple solutions [19,43,47], generating a population of results that are evaluated in each iteration step. Most recently, GA has been combined with HA to quickly evaluate triangular, strut-based structures to minimize compliance with volume constraints for a planar lattice design [43]. Despite its demonstration of feasibility for 2D cases, converting the framework to 3D may lead to difficulty, such as premature convergence when employing HA to reduce the number of design variables [47]. As an alternative, SA is not dependent on population size as it only evaluates one generated state (population size of one) per iteration step. It has also

been applied to heat transfer problems to find the optimal configuration of a finite number of components [41]. SA works to achieve a globally optimal solution by controlling the search based on heuristics modeled after metal annealing [48]. A major advantage of this optimizer is its ability to accept inferior designs based on a probability of acceptance, which is dependent on the current stage of the optimizer (e.g., the exploration stage). This allows for the optimizer to reverse out of local optima, even at later stages in the optimization process. Despite its potential, SA has not been applied to the design of lattice support structure design for LPBF. One potential reason is that only small perturbations are made within the design domain per iteration step for traditional SA optimizer methods [48]. For the design of lattice support structures with hundreds of design variables, changing one design variable per iteration step limits the region of exploration within the total design domain. Therefore, the traditional SA optimization method needs to be modified to efficiently explore the design domain for lattice support structure design.

2.4. Methodology

A new optimization method is introduced in this section for lattice support structure design. To this end, an overview of the problem is presented. Notably, the entire method is programmed in Python using a customized SA algorithm to perform optimization and a commercial Finite Element solver, ANSYS APDL, is utilized for thermal evaluations using the pyAPDL interface. The method, following the flowchart illustrated in Figure 1, is then described in detail beginning with the pre-processing procedure for optimizer inputs, including the design variables, boundary conditions, and optimizer hyperparameters. Next, the

stage-dependent annealing swapping strategy is explained before the evaluation of the proposed objective function. Finally, the optimization process is described.

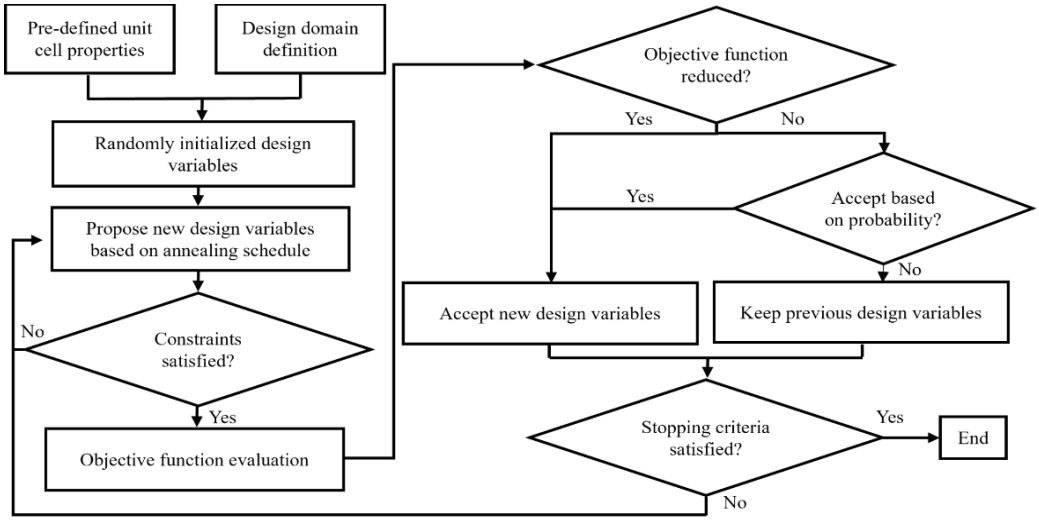

Figure 1: Flowchart of the proposed simulated annealing optimizer method for thermally conductive support structure.

The cantilever beam is a commonly used benchmark for the design of support structures and is employed here to introduce this method. Notably, the method established in this section is generally applicable to the design of other support structures. When heat is applied to build the cantilever, the lack of support underneath the large overhang results in non-uniform heat distribution and high accumulation of heat [34,35]. As shown in Figure 2, the volume underneath the overhang, the boundary defined by the dashed lines, is denoted as the design domain. By reconfiguring the distribution of individual unit cells, selected from a library, the heat transfers from the applied heating to the base plate, located at the bottom plane of the cantilever. In addition, the support structure generated within the design domain must also satisfy multiple user-defined manufacturing constraints.

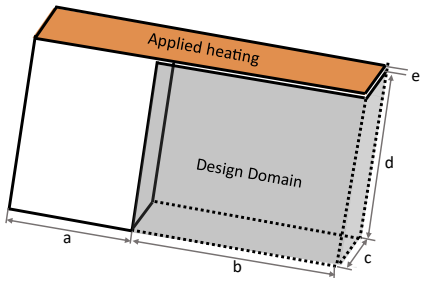

Figure 2: Geometry of the cantilever beam (solid lines) with the design domain (dashed lines) and variable dimensions.

2.4.1. Problem Overview

To begin formulating the optimization problem, the objective function is defined. The metric employed for this study to represent the heat dissipation (i.e., the diffusion of heat flow) is the minimization of the heat transfer rate through the base plate, Q_{out}, described in Section 2.4.4 and represented as Equation (1). The heat dissipation performance metric, Q_{out}, is chosen here for demonstration purposes as it is a practical measurement as opposed to the commonly employed thermal compliance [49]. Therefore, to minimize Q_{out} is to maximize the dissipation through the system. Other metrics also could be employed in practice based on users' preferences. The optimization problem is formalized as:

$$\begin{aligned} \text{find} \quad & x = [x_1, x_2, \ldots, x_n] \text{ to} \\ \text{minimize} \quad & Q_{out} = Q(x), && (1) \\ \text{subject to} \quad & KT = G, && (2) \\ & V(x) < \varepsilon_V * V_{max}, \text{ and} && (3) \\ & A(x) < \varepsilon_A * A_{max}, && (4) \end{aligned}$$

where $x_i \in [SC, BV, FC]$, $i \in \{1,2,\ldots,n\}$ and n is the number of geometric design variables. The design domain is evenly discretized to fit the bounding volume of the unit cells; however, the domain can also be partitioned to accommodate design variables with different bounding volumes [21]. The design variables, described in Section 2.4.3, have predefined geometric (e.g., strut size and orientation) and thermal properties to be leveraged by the optimizer to minimize the objective function subject to the defined AM constraints.

An applied constraint is the steady-state heat equation, Equation (2), for which K is the heat conduction matrix and G is the internal heat generation vector containing heat sources and boundary conditions, explained in Section 2.4.2. Other constraints of interest regarding the AM process chosen for this demonstration are volume (V(x)) and contact area with the part (A(x)), Equation (3), and Equation (4), respectively. In addition to these constraints, users may consider other design requirements related to the design variables such as uniformity of temperature distribution along the top surface [12] or residual deformation [16,18]. Volume is a commonly used constraint as the support structure is material waste after the part has been removed from the build plate [8,26]. The less material required for the sacrificial material typically results in reduced build cost and build time [9]. Therefore, the optimizer must consider a fraction, ε_v, of the total volume of the design domain, V_{max}. Regarding the contact area, post-processing is also imperative to the design of parts for the build. If support structures are not removed properly, the residue can increase the surface roughness of the part [1,35,46]. For more delicate features such as thin-walled designs, removing excess material from the surface could damage the part [50]. A fraction, ε_A, of the sum of the areas of the part within the design domain on the XY and YZ planes, A_{max}, is considered.

2.4.2. Defining Design Domain and Boundary Conditions

Before the optimization procedure can be run, the design domain must be defined. Hence, a full transient thermal simulation is performed within the pre-processing procedure to obtain input for the optimization model for the cantilever void of support structure. As opposed to a computationally expensive exact solution to heat source input that considers scan pattern and other phenomena associated with the melt pool, the flash method is employed for the layer-by-layer simulation [18,31,51] using commercial FEM solver, ANSYS APDL. Details regarding the equations to solve the two-step procedure of heating and cooling of activated elements to simulate the layer-by-layer simulation can be found in work by Li *et. al* [31].

To begin the layer-by-layer simulation, the column of height *d* contains all active elements whereas the overhang elements of height *e* are deactivated. For the first heating cycle, a superlayer of elements

composed of multiple actual powder layers is activated with a volumetric heat flux at the surface nodes, shown in Figure 3. To calculate the amount of volumetric heat flux, q", the following equation is applied:

$$q" = (A_b \cdot P)/(d_m \cdot d_s \cdot h), \quad (5)$$

where A_b is the laser absorptivity, P is the power, d_m is the depth of the melt pool, d_s is the spot diameter and h is the hatch space [31]. After heating is applied for a user-defined time, the cooling occurs to simulate the amount of time for the recoater to apply another layer [30]. The cycle of heating and then cooling continues until all overhang element layers have been activated. The base plate is represented as the heat sink and is kept at a constant temperature with an applied convection coefficient [31]. Although the material properties are temperature-independent, to account for the heat loss due to convection and radiation, a convection coefficient is applied to the sides of every activated layer [31].

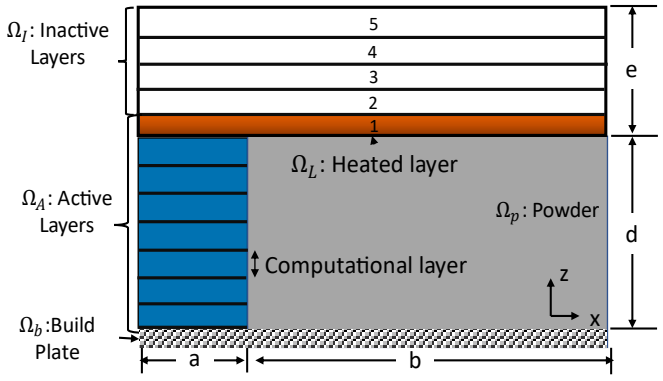

Figure 3: 2D schematic of a cantilever beam showing an example of a model of the layer-by-layer process simulation.

Layers for which the temperature distribution becomes most non-uniform are the layers of the build that need a support structure. The temperature distribution of the non-uniform layer is extracted from the simulation to be used as boundary conditions for the steady-state evaluation, described in Section 2.4.4.

2.4.3. Choosing Design Variables

As opposed to a continuous distribution of material elements, pre-defined unit cells, chosen from a library, are selected as the values of design variables. The size of the library can make a difference in the types of constraints that can be considered and the size of the design solution space. A large library would

enable multiple constraints, such as printability and functionality, to be easily obtainable. Commonly designed unit cells are honeycomb [4,52] and octet truss [4,53–56]. However, for this problem, the design exploration would increase exponentially as there are m^n possible configurations, where *m* is the number of pre-defined unit cells and *n* is the number of design variables [53]. Therefore, proper selection of the unit cells can be obtained by establishing guidelines, such as manufacturability [55,57] and connectivity [57–59]. Manufacturability refers to both the individual unit cell and the entire lattice. It considers the capabilities of the printer to fabricate specific geometries (e.g., maximum overhang angle and minimum strut size). Connectivity refers to the connection between one unit cell to another. Disconnected unit cells can result in a build-up of intracellular stress or even part failure [55]. Therefore, there exists a trade-off between computational complexity and constraint consideration that must be carefully considered by the designer when choosing the optimization process [53]. Therefore, this demonstration uses three commonly employed strut-based unit cells for the library, shown in Figure 4: simple cubic (SC) [4,18,37,38], body-centered vertical strut cubic (BV) [19,60], and face-centered cubic (FC) [4,40,60]. Other types of unit cells also could be included in the library when the optimization method introduced in this section is implemented in practice. Each self-supporting cell occupies a $2\times2\times2$ mm^3 space and can be manufactured with a minimum strut diameter of 200 microns [56]. As shown in Table 1, each unit cell has properties that are advantageous to the flow of heat, the volume, or the amount of area connected to the part, shown in bold. SC has a low volume but has a relatively large contact area and a low thermal conductivity, as described in Section 2.4.4. In contrast, FC has the highest volume, highest thermal conductivity, and asymmetric contact area properties. BV possesses intermediate thermal properties and volume while having the lowest contact area for both the XY and YZ planes.

Table 1: Properties of various unit cells for AlSi10Mg in comparison to equivalent solid volume. Advantageous qualities in bold.

Unit Cell	K_{eff} [W/m°C]	Volume [mm^3]	$Area_{XY}$ [mm^2]	$Area_{YZ}$ [mm^2]
Solid	110	8	4	4
SC	12.37	1.82	2.31	2.31
BV	24.39	2.82	0.567	1.30
FC	39.43	3.69	0.846	3.24

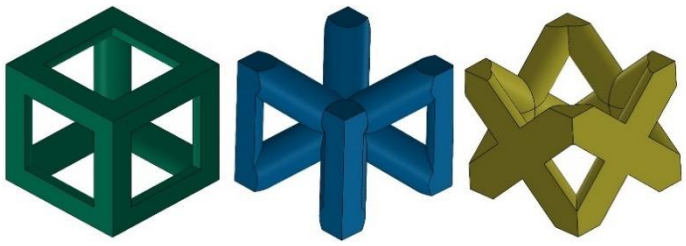

Figure 4: Unit cells employed for lattice support structure heat transfer analysis (from left to right): simple cubic (SC), body-centered vertical strut cubic (BV), and face-centered cubic (FC)

2.4.4. Evaluating Objective Function

Running a transient model during each iteration for each layer leads to high computational costs, despite the combination of single-layer activation and superlayers [18,30,61]. To combat the high computational cost, a transient model can be performed with an applied distributed, effective heat source in one timestep that varies spatially and temporally [18]. However, if the accuracy of the model is imperative, particularly when more complex models are evaluated, this can greatly increase the computation time when utilizing fine elements. Alternatively, a steady-state model can be performed within one step [30,51]. LPBF can be simplified to a system of two parallel plates in which heat moves from one plate (source) to another (sink) [28]. Lattice support structures are employed for the transfer of heat from the source to the sink underneath the cantilever beam. Using ANSYS-Python interface, pyAPDL, the input boundaries for this approach are the temperature distribution obtained from the transient model to evaluate, from Section 2.4.2. This approach is compatible with simple and complex designs [51]; therefore, it will be used in this study for evaluation of the minimization of the heat transfer rate through the base plate. In this model, only heat conduction is considered.

The governing equation for this model is

$$q''=\nabla\cdot(K_{eff}(x)\nabla T(x)), \quad (6)$$

where q" is the internal heat generated by the system, K_{eff} is the effective thermal conductivity, and ∇T is the temperature gradient. To relate the dissipation of heat to a steady-state model, Fourier's heat conduction law,

$$q' = -K_{eff}\, dT/dz, \quad (7)$$

is evaluated as it relates the rate at which heat flows through any surface per unit area, q', with the conductivity, K_{eff}, the temperature difference between the surfaces for the cantilever height of *z*. More specifically, the heat transfer rate, Q_{out}, is calculated by integrating the flux over the area of the element [41]. This problem is numerically solved using the commercial finite element analysis solver, ANSYS.

Given the complexity of the many possible unit cells and configurations within the design domain, a new mesh needs to be generated for each iteration during optimization. An alternative is to use a simpler representative volume with equivalent material properties, namely, the homogenization approximation [62]. The basic idea behind the approach is that the effective (i.e., average) properties of an RVE can be found by mapping the relationship between the entire domain composed of many RVEs to a single RVE (i.e., unit cell). This requires solving two physics problems, one at the macroscale and one at the microscale, that are coupled by a scaling factor. Two assumptions are made with this approach: (1) the RVE chosen is infinitely small compared to the macroscopic domain, and (2) periodic conditions apply within the macroscopic domain. This procedure has been previously employed in optimization problems to reduce the computational effort for functionally graded [18,37,38,63] and non-graded [43,64,65] lattices. More information can be found in a review performed by *Hassani and Hinton* [62].

2.4.5. Performing Optimization Process Based on SA

The modified SA-based method begins with a randomized distribution of SC, BV, and FC unit cells that fill the void design domain at the initial state. The method starts to fill the design domain by randomly selecting an initial unit cell to be placed at an initial datum point, in this case, the far left-most corner in

Figure 2. Next, another cell is added in relation to the previous cell, given that it is within the boundary and does not overlap an existing cell position, and the counter tracking the number of possible cell positions increases incrementally. If the proposed move violates boundary or overlap constraints, the move is rejected without increasing the counter and another random cell is selected. To continue the build, a random cell from the existing structure is selected and the action of assembly is continued until all possible positions are generated (i.e., the cell counter reaches the maximum number of possible positions). With the initial state completed, the state is evaluated and recorded.

The initial state is progressively altered iteratively according to the future evaluations of the objective function at a rate defined by the user in the pre-processing stage. The starting temperature, T_0, is defined to initiate the optimization. Further temperature reduction follows the geometric cooling schedule defined as

$$T_{k+1} = \alpha \times T'_k, \tag{8}$$

where T'_k is the annealing temperature at the k-th state, T_{k+1} is the temperature at the next state and α is the cooling constant [41]. The probability of acceptance is defined as

$$P_{acc} = exp(-(E_2 - E_1)/T'_k), \tag{9}$$

where E_k and E_{k+1} are the energy states (i.e., objective functions) of the previous state and current state, respectively. To determine the acceptance, the computed probability, P_{acc}, is compared to a randomly generated number between 0 and 1. If P_{acc} is greater than the random number, the inferior design state is accepted; otherwise, it is rejected.

One limitation of the traditional SA method is that it evaluates changes from small changes in the design variables per iteration. With a large design space within the design domain for the lattice support structure, it would be inefficient to optimize by performing only a couple of moves (i.e., swap of a unit cell for another randomly chosen unit cell) per iteration given that there are 3^n possible configurations, based on the number of design variables (n). Therefore, to encourage a wider search of the design solutions for practical application, an added modification is the number of swaps per iteration that is made to be

dependent on the annealing schedule, entitled stage-dependent annealing swapping strategy. During the initial stages, a rigorous exploration occurs by setting the number of swaps equivalent to n. As T'_k decreases to 1/5th of T_0, the number of swaps decreases to $n/10$. In the final stages of the design, when T'_k is less than 0.5, the number of swaps decreases to one per iteration. These values are selected as they create a steep descent in the objective function. Further study will be needed to investigate other strategies for swapping based on the objective function or the annealing schedule. The stopping criteria of this optimizer can be when T'_k reaches the minimum temperature [66], the difference in objective function between subsequent iterations is less than a value [67], or a number of iterations [68,69]. For this demonstration, the stopping criteria is chosen as a minimum T'_k of 0.1, which has been shown in literature to have a high convergence speed [66]. Notably, this method is programmed using custom Python code to run SA optimizer which called pyAPDL for simulation-informed evaluations of the objective function.

2.5. Case Study of Cantilever Beam

A case study of a cantilever beam, shown in Figure 2, is employed to validate the modified SA-based method introduced in Section 3. The proposed method begins with defining the design variables, boundary conditions, and hyperparameters for the optimizer. Once established, the initial design is generated by filling the void of the design domain with a randomized configuration. The objective function is evaluated using the homogenization approximation for the initial design to begin the optimization procedure. Each iteration, a stage-dependent number of swaps occurs before evaluating the objective function. When the stopping criteria is reached, the results are compared to the homogenous benchmark support structures for the steady-state and transient simulations. The results of the case study indicate that by applying the proposed framework, an optimally directed thermal performance can be achieved with AM constraints satisfied.

Pre-processing is required for the initialization of the optimizer. To identify the design domain for supports and the boundary conditions for the time-efficient steady-state model, a transient thermal FEM simulation is performed. Layer-by-layer simulation is an efficient part-scale thermal heating approach as it

saves computational time while still capturing the temperature trends [31]. The dimensions of the cantilever beam for the problem defined in Figure 2 are: a = 4 mm, b = 18 mm, c = 10 mm, d = 10 mm, e = 1 mm. The finite element mesh is composed of 105,000 hexahedral elements of uniform size: 0.2 mm^2. Since the area of interest is the temperature underneath the overhang, the elements within the vertical column until height d are assumed to be fully cooled to room temperature, as shown in Figure 3. Within the simulation, they are active at the start and then each superlayer of 0.2 mm is activated, corresponding to approximately 7 real powder layers.

By applying the respective process parameters (Table 2) on the surface of the recently activated layer, the averaged y-axis distribution along the x-axis of the cantilever after heating is shown in Figure 5. The five layers of the overhang correspond to the layers labeled in Figure 3. The results show that after heating the first superlayer, the temperature along the x-axis exhibits a large jump in temperature from the column directly connected to the base ($x < 4$ mm) to the overhang ($x \geq 4$ mm). This is expected within LPBF as the temperature will be significantly higher above the powder because the heat does not have anywhere to dissipate [30,34]. The following heated layers have a reduced temperature distribution in comparison to the first layer, especially the last layer, similar to trends found in literature [30]. Since the heat is uniformly applied across the top, the temperature has a steep and abrupt slope rather than no slope, which would imply uniform heating. When the second layer of heating is applied, the thermal gradient is higher than the first near the end ($x \geq 13$mm). This indicates that the structure is not sufficiently cooled enough for another layer of powder to be properly deposited and build failure would occur, such as the formation of dross on the down-ward-facing side [34] or damage to the recoater blade when applying another layer. Therefore, the support structure is needed to quickly dissipate heat from the overhang to the base. For this study, the temperature distribution across the top of the cantilever for the first layer will be utilized as the applied load for the design domain in the steady-state optimizer evaluation.

Table 2: Parameters for layer-by-layer application [31]

Process Parameter	Value
Volume heat flux, q" [W/m^3]	2×10^{13}
Convection coefficient for heat loss to environment, h_{side} [W/m^2°C]	400
Convection coefficient for heat loss to build plate, h_{plate} [W/m^2°C]	8,000
Heating time per layer, t_h [s]	6×10^{-4}
Cooling time per layer, t_c [s]	5
Build plate temperature, T_{amb} [°C]	20

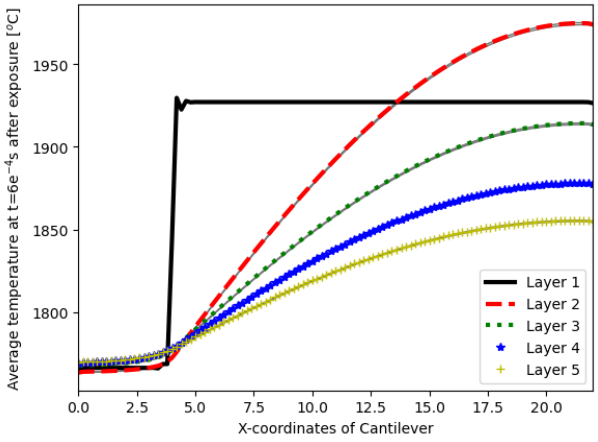

Figure 5: Temperature transition of the LPBF process: represents temperature at the end of the heating cycle for all the computation overhang layers.

The last components of the pre-processing steps are performed based on the results from the transient thermal simulation about the design domain. For this demonstration, the design domain is evenly partitioned to allow for a total of 225 geometric design variables. SC, BV, and FC are the uniformly sized unit cells chosen possessing properties outlined in Table 1. The pre-processing stage concludes by defining the main hyperparameters cooling schedule for the annealer as $T_0 = 50$ and $\alpha = 0.5$.

The components from the pre-processing step are inputted into the system to begin the optimization. First, the initial randomized configuration is generated to fill the initially void design domain. The goal of the optimizer is to maximize the heat dissipation (i.e., diffusion of heat flow) through the lattice support structure. A steady-state model is chosen to evaluate the heat flow through the lattice support structure only by conduction from the overhang to the base. The constraints on volume and area are selected as V_{max} =

750 mm^3 and A_{max} = 140 mm^2, respectively. These constraints are chosen to demonstrate how the optimizer may be tuned according to the advantages of each of the unit cells without restricting the design space to a single unit cell configuration. For future applications, practitioners may specify these constraint values based on manufacturing cost and post-processing requirements.

The homogenization approximation allows for the representation of a block-like structure (i.e., RVE) that is meshed into 0.25 mm^3 hexahedra. By combining the stage-dependent annealing swapping strategy coupled with the homogenization approximation, the iteration curve appears to have reduced the heat transfer rate of the lattice support structure from its initial state, shown in Figure 6, within 1,400 iterations, equivalent to the number of function calls. A reduced Q_{out} corresponds to a higher dissipation of heat through the system. The optimizer is run 30 times to obtain a statistical average and standard deviations of 1 sigma. Using a desktop computer, Intel Core i7-7700 CPU, each run is approximately 5 hours per simulation resulting in about 12 seconds per iteration. For this size of a simulation, employing the microscopic material distribution with SIMP for optimization would take significantly longer.

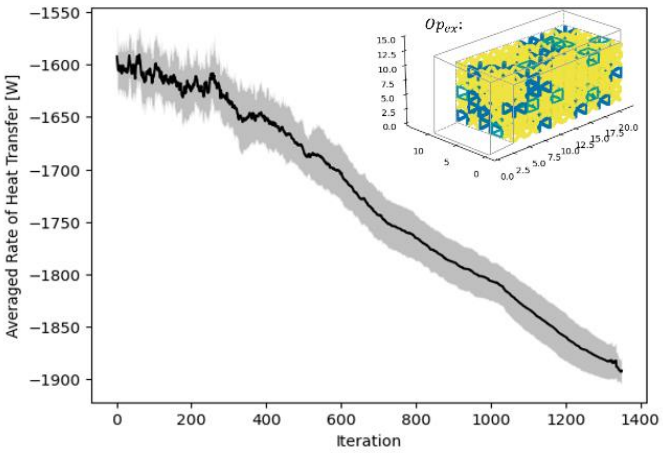

Figure 6: Average objective function value for heat transfer rate with shaded regions showing standard deviation with an example, Op_{ex}, configuration with final values: Objective = -1,900 W, Volume = 615 mm^3, Area = 106 mm^2.

The results from the optimization, shown in Table 3, compare the average of 30 computationally designed designs, Op_{avg}, to the benchmark designs. Starting from a randomized initial state, the optimizer is capable of producing unit cell configurations that have better dissipation than BV Only and SC Only lattice support structures, for both the exact model ($Q_{in,exact}$) and homogenization approximations ($Q_{in,h}$), as

shown in Table 4. The dependency on the initial configuration that is typically found using gradient-based optimizers [32,37] is not found in this approach as there is convergence of the objective function within a relative standard deviation of 0.7%. A limiting factor of this approach is that the predefined library constrains the bounds of achieving better properties than a homogenous structure composed only of the best unit cell property, (e.g., best contact area for BV Only). However, the optimizer leverages the favorable properties of each unit cell to achieve a lattice support structure with an acceptable objective function within the pre-defined constraints. Of the three benchmark lattice structures, BV Only is the only structure that satisfies the predefined constraints, due to its intermediate properties. When compared to BV Only, the heat output of Op_{avg} (absolute value) is 16% higher. Based on the computationally designed steady-state model, Op_{avg} balances the tradeoffs of the unit cell properties to generate better macroscopic thermal properties for steady-state thermal analysis. Furthermore, it should be noted that heat transfer through the solid column is utilized for all configurations (up to height *d*). The exact fraction of flow through the solid domain versus the support structure domain was not computed and could be included in future work. However, it is expected that with the applied non-uniform temperature distribution and 81% of the area belonging to the support structure, most of the heat is flowing through the support structure.

Table 3: Comparison of the benchmark results to the average of computationally designed structures, Op_{Avg}, with standard deviations shown in parentheses for the optimizer.

	$\|Q_{in}\|$ [W]	Volume V(x) [mm^3]	Area A(x) [mm^2]	SC/BV/FC	Constraint Satisfaction V(x) < 750 A(x) < 140
Solid	4,546	1,800	280	0/0/0	No
SC Only	1,196	409	161	225/0/0	No
BV Only	1,607	634	57	0/225/0	Yes
FC Only	2,124	830	120	0/0/225	No
Op_{Avg}	1,887 (15.0)	745 (5.56)	108 (4.94)	18/58/149 (3.23/5.43/5.34)	Yes

Although a steady-state thermal analysis is employed during the optimization, LPBF is a transient thermal problem; therefore, a transient solution is still needed to assess the time-dependent transfer of heat through the system. A full-scale transient thermal analysis for the application of the first layer is run to further validate the computationally designed results. The metric chosen to compare the computationally designed structure to the benchmark designs is the time taken for the entire structure to converge to a stable temperature within a 1% difference. All maximum temperatures in the system are reduced to below the melting temperature of AlSi10Mg for both the benchmark and optimal designs; however, the rates at which they cool are just as important in producing stable designs [18]. Table 4 shows that SC Only structure takes the longest time to reach a steady-state temperature at 3.28s. This is attributed to its horizontal surface and low volume. The heat flowing through the horizontal struts encounters a disruption in vertical flow; therefore, the heat must flow out to the vertical struts, causing an accumulation of heat [60]. However, the presence of the vertical struts makes BV Only more advantageous as it provides a direct path of heat flow down to the base plate [40]. However, its small volume prevents it from achieving dissipation rates as high as Op_{ex} and FC Only. With the highest volume, FC Only dissipates the heat the fastest; whereas Op_{ex} achieves steady-state the second fastest at 1.45s. These results indicate that the method achieves desirable

properties for thermally conductive lattice support structures while adhering to AM constraints for the transient and steady-state cases. More specifically, by setting the objective to minimize heat transfer rate into the system for the steady-state thermal analysis, heat dissipation can be maximized for the transient-thermal analysis.

Table 4: Comparison of the benchmark results to a randomly selected computationally designed structure, Op_{ex}, for steady-state heat flow exact and homogenization approximation results and transient exact solution time results.

Analysis Model	Simulation	SC Only	BV Only	FC Only	Op_{ex}
Steady-state	$Q_{in,h}$[W]	-1,196	-1,607	-2,124	-1,608
	$Q_{in,exact}$[W]	-1,198	-1,605	-2,132	-1,647
Transient	t_s[s]	3.25	2.18	1.38	1.45

2.6 Conclusions

Optimizing support structures for Laser Powder Bed Fusion (LPBF) is an important field of research as they are vital to the fabrication of parts, particularly those with overhangs. The main contribution of this work is a modified SA-based method that generates lattice support structures. The method the computational bottlenecks associated with non-gradient-based optimization. To this end, stage-dependent actions are coupled with equivalent static loading and homogenization approximation for the SA-based optimizer. Results show that the optimal hybrid lattice structures produce 16% better heat transfer rates than the benchmark structure with predefined additive manufacturing (AM) constraints satisfied (BV Only) by leveraging favorable properties from multiple unit cells.

This study is the first step in broadening the application of stochastic optimizers within the interdisciplinary topic of AM. The modified SA-based optimizer allows for the use of physically explainable objective functions and a library of manufacturable, self-supporting structures that do not need to be differentiable to perform the sensitivity analysis. It also provides a systematic approach to further

explore the design space while circumventing time-consuming evaluations of the physics-based objective function. From a practical application standpoint, in which tracking the costs of the build is imperative, this method enables designers to control costs during the build and post-processing portions. These values are represented in this study as volume and contact area, respectively, but can be further refined for other applications.

3. Chapter 3: An Optimally Directed Lattice Support Structure Design Method For Heat Dissipation and Structural Integrity in LPBF[2]

3.1. Overview

Given the multi-functionality of support structures, heat dissipation and structural integrity must be considered when designing lattice support structures. Therefore, the proposed modified, simulated annealing-based method is expanded to design optimally directed lattice support structures to maximize heat dissipation while adhering to user-defined manufacturing constraints, such as residual stress and deformation. This model incorporates two sub-models that predict the thermal and mechanical properties of the structure due to the change in unit cell distribution. Two case studies are considered in this demonstration of the method: a cantilever beam and an aerospace bracket. The additional study of an aerospace bracket considers a higher dimensional problem with multiple design domains to demonstrate the practical application of this method. The results of these case studies show the method's ability to achieve material cost savings of up to 61% and post-processing cost savings of up to 62% when compared to a solid support domain while satisfying manufacturing constraints.

3.2. Introduction

Additive manufacturing (AM) has been repeatedly proven to fabricate intricate components that were difficult to create using any other method within various industries [1,4], such as the design and fabrication of lightweight control sticks for the aerospace industry [70] and suspension system parts for the automotive industry [71]. This is particularly apparent in the creation of metal components using the commonly employed process of Laser Powder Bed Fusion (LPBF). By iteratively spreading microscopic layers of metal powders, a high-power energy source melts the desired cross-section for each layer to create the final part [1,2]. When manufacturing with LPBF, it is imperative to incorporate support structures within the

[2] L. White, X. Liang, G. Zhang, J. Cagan, Y. J. Zhang. Designing Thermally Conductive Lattice Support Structures Constrained by Residual Stress and Deformation for LPBF. In Review for *Journal of Computing and Information Science in Engineering*. 2023.

build for its success, particularly for components with overhang features. Overhangs are downward-facing surfaces, less than 45° with respect to the build plate, that are greater than 5 mm [10,11] in length. In part due to the low conductivity of the metal powder [12,34], when overhangs void of support structures are created, deformities to the part (e.g., part distortions [16,18,31–33], discoloration [26], high surface roughness [2,34,35]) and damage to the machine due to collision between the part and the powder re-coater [2] are likely to occur. In such cases, support structures are required to both anchor the part to the build plate and to help dissipate heat [10–13]. However, utilizing support structures will increase manufacturing costs, which can be significant given the high cost of the metal powder [9].

In order to manufacture complex geometries with overhang features using LPBF, lattices are a feasible solution for the fabrication of support structures [10,11,32]. Lattices are composed of individual unit cells that are either periodically or non-periodically distributed. These structures are promising because they reduce manufacturing costs by lowering material waste, possess tailorable mechanical and thermal properties, are self-supporting, and are suitable for convenient powder removal [10]. Thus, extensive research has been conducted to optimize discrete unit cell designs manufactured using AM [13,16,18,28,44,50,61]. Specifically for thermal applications, these optimization efforts are typically approached using gradient-based optimizers [36]. However, utilizing topology optimization with gradient-based optimizers for distinct design variables can be challenging [41,42], especially with the added complexity of the sensitivity equations [18] and initial design dependency [32,37]. These challenges are in part attributed to the required differentiable objective function and the limited design domain exploration. An alternative approach is to employ non-gradient-based optimizers, such as genetic algorithm (GA) and traditional simulated annealing (SA), to design lattice support structures. These non-gradient-based optimizers allow for an increased design domain exploration, and they do not rely on the differentiation of the objective function [42]. Unfortunately, expensive computation has been one bottleneck preventing their application to the design of lattice support structures. For lattice support structure design in LPBF, the high computational cost of existing non-gradient-based optimizers is attributed to both the cost to evaluate

simulation-based objective functions and constraints (e.g., through expensive thermomechanical analysis using finite element solvers) in a single iteration and the cost to explore the design domain through a large number of iterations.

Based on the limitations of existing optimization techniques for lattice support structure design, a modified SA-based method is introduced in this paper to maximize heat dissipation of the lattice support structure while adhering to manufacturing constraints. Modifications to the traditional SA optimizer have been made to address the computational bottleneck associated with the cost to execute simulation-based evaluations at each iteration and the high iteration count required for design domain exploration. Specifically, homogenization approximation and equivalent static loading are integrated into the method to quickly evaluate multi-physics sub-models at each iteration step during the design optimization process. Furthermore, a stage-dependent annealing swapping strategy is created and employed by the method to derive the optimal distribution of unit cells within a reasonable number of iterations.

The remainder of this chapter is organized as follows: related work of support structure design for LPBF and limitations of extant approaches are discussed in Section 3.3. Section 3.4 introduces the modified SA-based method for lattice support structure design optimization. The method is validated through two case studies of a cantilever beam and an aerospace bracket in Section 3.5. Section 3.6 draws the conclusion and points out future work.

3.3. Background and Related Work

Support structures are critical for heat dissipation and anchoring the part within LPBF. This is particularly important when designing structures with overhangs, for which the heat can quickly accumulate along the unsupported regions leading to undesirable properties, such as distorted parts [16,72–74] and dross [2,34,35]. Existing gradient-based optimization methods to design lattice support structures are summarized with regard to progress and remaining challenges. Non-gradient-based optimizer methods are then summarized. The focus of this brief review is on the application of lattice support structures for heat

dissipation. Detailed reviews of heat structure design, unit cell design, and support structures can be found in publications written by *Dbouk* [36], *Nazir et al.* [4], and *Jiang et al.* [8], among others.

To capture both the non-uniformity and the time-dependency of heat dissipation, recent work has considered the transient temperature effects for the dissipation of heat and the mechanical properties [18]. Evaluation of the macroscale lattice is accelerated by coupling a library composed of the relative densities of a simple cubic structure's effective properties with the HA, which employs RVEs [16,18,37,43]. This drastically reduces the number of design variables from microscale material elements to mesoscale unit cells to choose for each possible location [16,18,37,44]. By utilizing a gradient-based optimization method, the model was able to reduce the liquid lifetime (i.e., the amount of time the top layer is above liquid temperature) and reduce the residual deformation by 42% when compared to the benchmark of a uniformly sized simple cubic lattice support structure. However, only a simple cubic unit cell was optimized for the density, limiting the optimizer's ability to consider more AM constraints, such as reducing contact area to reduce post-processing costs [1,35,45,46].

As an alternative, non-gradient-based optimizers, such as traditional simulated annealing (SA) and genetic algorithm (GA), are reputable for optimizing problems with discrete design variables [41,42]. Both SA and GA use a stochastic optimization approach that allows for a broader search of the design domain, overcoming potential local optima. GA is based on Darwinian evolution to find one or multiple solutions [19,43,47], generating a population of results that are evaluated in each iteration step. Most recently, GA has been combined with HA to quickly evaluate triangular, strut-based structures to minimize compliance with volume constraints for a planar lattice design [43]. Despite its demonstration of feasibility for 2D cases, converting the framework to 3D may lead to difficulty, such as premature convergence when employing HA to reduce the number of design variables [47]. As an alternative, SA is not dependent on population size as it only evaluates one generated state (population size of one) per iteration step. It has also been applied to heat transfer problems to find the optimal configuration of a finite number of components [41]. SA works to achieve a globally optimal solution by controlling the search based on heuristics modeled

after metal annealing [48]. In the previous chapter, a new method based on a modified SA to generate lattice support structures by dissipation of heat was proposed. However, given the multi-functionality of support structures, improvements are necessary. In this chapter, the previously established method is expanded to incorporate residual stress and deformation that accrue due to thermal distortion.

3.4. SA-Based Method for Lattice Structure Design

According to the research gap presented in Section 3.3, a modified SA-based method is introduced in this section to design lattice structures constrained by AM requirements (e.g., stress, deformation, support removal, and volume limitation) for support structure design. By utilizing HA and equivalent static loading (ESL), the multi-physics problem of LPBF is quickly evaluated per iteration step. In addition, efficient design exploration is achieved by incorporating a stage-dependent annealing swapping strategy in the design optimization process. To this end, a flow chart for implementing the proposed method is shown in Figure 7. Notably, the entire method is programmed in Python using a customized SA algorithm to perform optimization and a commercial Finite Element Method (FEM) solver, ANSYS APDL, is utilized for thermal and structural evaluations using the pyAPDL interface. ANSYS Material Designer is also used to compute the homogenized material properties of the unit cell library.

There are three major steps included in the flow chart. The problem statement is first formulated with the chosen geometry and design variables. Next, process analysis is performed using two commonly employed part-scale models to obtain the ESLs. After completing all the pre-optimization work, the modified simulated annealing-based optimizer is run until the stopping criteria is satisfied. Finally, the computationally designed result is evaluated using the part-scale models to validate the approximations. Notably, the method presented in this section could be applied to the design optimization for LPBF with any user-defined objective function and constraints.

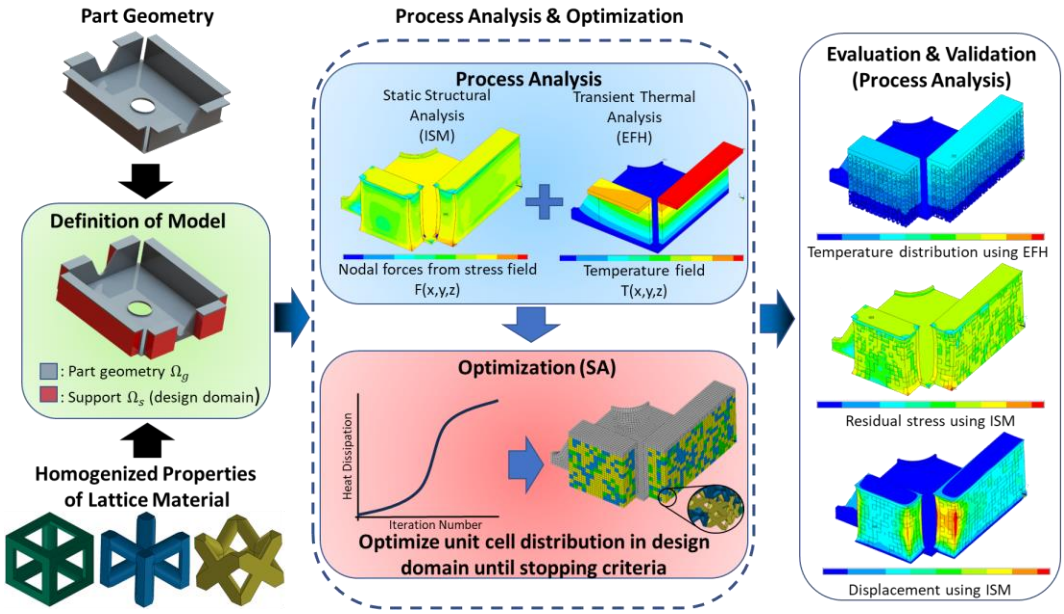

Figure 7: Flowchart summarizing the proposed optimization methodology with part-scale LPBF sub-model simulations for the design of computationally designed lattice support structure for a quarter of an aerospace bracket.

3.4.1. Problem Overview

A quantifiable objective function, design variables, and corresponding constraints are first defined for the design optimization problem. For this study, the method is applied to the design of lattice support structures for LPBF. The multifunctional design of support structures increases the computational effort in solving non-linear, multi-physics equations. To demonstrate the proposed method's ability to efficiently combat this challenge, two case studies are considered for which support structures are imperative for the printability and final part quality: a simple cantilever beam (Figure 2(a)) and an aerospace bracket (Figure 2(b)). In both cases, when heat is applied to the build part, the lack of support underneath the overhangs results in non-uniform heat distribution and high accumulation of heat [34,35]. The cantilever beam is a commonly used benchmark for the design of support structures [13,16,18,74] whereas the aerospace bracket [73], is investigated due to its high dimensionality and multiple design domains. Furthermore, the overhang for the cantilever beam is long compared to the overhang of the aerospace bracket, which may affect the design configuration the optimizer finds as a solution. As shown in Figure 2, the volume underneath the overhangs, depicted in dashed lines, is denoted as the design domain for the lattice support structure.

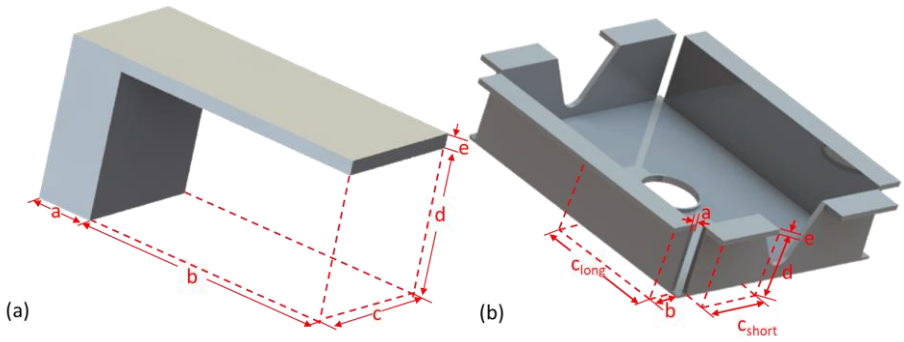

Figure 8: 3D representation of the two cases with dimensions: (a) cantilever beam and (b) aerospace bracket

To begin formulating the optimization problem, the design objective function is defined. The metric employed here to represent the heat dissipation (i.e., the diffusion of heat flow) is the minimization of the heat transfer rate into the system Q_{in}, described in Section 3.4.4 and represented as Eq. (10). The heat dissipation performance metric, Q_{in}, is chosen here for demonstration purposes as it is a practical measurement as opposed to the commonly employed thermal compliance [49]. Other metrics also could be employed in practice based on users' preferences. The optimization problem is formalized as:

$$\begin{aligned} \text{find} \quad & x = [x_1, x_2, \ldots, x_n] \text{ to} \\ \text{minimize} \quad & Q_{in} = Q(x), && (10) \\ \text{subject to} \quad & KT = q, && (11) \\ & CU = F, && (12) \\ & \frac{\sigma_j^{PN}}{\sigma_y} \leq \sigma_{max}, && (13) \\ & U_{sum} \leq U_{max}, && (14) \\ & V(x) < V_{max}, \text{ and} && (15) \\ & A(x) < A_{max}. && (16) \end{aligned}$$

The design variables, x_i, are one of the unit cell types from the library with $i \in \{1, 2, \ldots, n\}$, where n is the number of possible locations for the unit cells. Each unit cell has pre-defined geometric properties (e.g., strut size and orientation) and thermal properties to be leveraged by the optimizer to minimize the objective function subject to the AM constraints. The design domain is evenly discretized to fit the bounding volume of the unit cells.

An equality constraint of the optimization problem is the weak form, steady-state heat equation, Eq. (11), for which K is the heat conduction matrix and q is the internal heat generation vector containing heat sources and boundary conditions [75]. Eq. (12) represents another equality constraint for the weak form static mechanical analysis, where C is the stiffness matrix, U is the displacement matrix, and F is the applied force [76]. The thermal model inputs are temperature boundary conditions from under the overhang whereas the mechanical model employs reaction forces as input, as explained in Section 3.4.2. Commonly utilized support structure structural properties include structural compliance [19,72,77], residual stress [16,21,72], or deformation [74,78,79]. In addition to the constraints described in this section, users may consider other design requirements related to the design variables such as uniformity of temperature distribution along the top surface [34]. For this study, stress constraints and deformation constraints are utilized simultaneously. Stress is considered by evaluating the maximum normalized von Mises stress within the structure ($\sigma^{vM}{}_{max}$), shown in Eq. (13) using the commonly employed P-norm stress constraint (σ_j^{PN}) [16,72,80]:

$$\sigma_j^{PN}(x) = \left(\frac{1}{N_j} \sum_{a \in \Omega_j} \left(\sigma_a^{vM}(x) \right)^p \right)^{\frac{1}{p}} \tag{17}$$

where N_j is the number of stress evaluation points in a set of Ω_j and p is the p-Norm factor. The stress level technique for p-Norm stress constraint utilized in this study clusters stresses with similar stress levels and compares each j number of clusters to the maximum stress value [80]. This approach allows for both a local and global analysis of the distribution of stress to prevent stress concentrations. Higher p-values result in more uniform stress distribution but may result in more iterations [80,81]. However, low p-values result in the average stress, e.g., $p = 1$. The stress of each cluster is normalized by the material's yield strength, σ_y, to avoid numerical inaccuracy.

Knowledge regarding how the build part deforms is critical during and after printing. During printing, large upward deformations greater than the layer thickness, L, may damage the re-coater when depositing another layer [74,78,79]. To account for the shrinkage of the powder when melted to a solid layer, a relative

powder density, ρ_{shr}, can be applied to calculate the maximum height of deformation [79]. The following equation formulates the maximum z-displacement:

$$U_z = L/\rho_{shr}. \tag{18}$$

After printing, part deformation is imperative to determine whether the part is within geometrical tolerance for functionality, particularly on the *XY* plane where distortion is most prevalent [31,82]. In the traditional manufacturing method of die-casting, a draft angle is a slight slant in the vertical direction of the cast that is used to aid in the removal of parts from a mold [83]. Large draft angles on the *XY* plane could make manufacturing using LPBF inefficient as opposed to other traditional manufacturing methods. Thus, the maximum deviation in the x and y-direction for the overhang will be the maximum distortion on the *XY* plane caused by the draft angle needed for parts that are cast. The total maximum deformation will be the magnitude of the maximum displacements in x, y, and z, as shown in Eq. (19). To obtain the stress and displacement within the system, boundary conditions are applied to a homogenized structure of equivalent dimensions.

$$U_{sum} = \sqrt{U_x^2 + U_y^2 + U_z^2}. \tag{19}$$

Other inequality constraints of interest regarding the AM process chosen for this demonstration are volume, $V(x)$, and contact area with the part, $A(x)$, shown as Eq. (15) and Eq. (16), respectively. Volume is a commonly used constraint as the support structure is material waste after the part has been removed from the build plate [8,26]. The less material required for the sacrificial material typically results in reduced build cost and build time [9]. Therefore, the optimization problem is constrained by a user-defined volume fraction constraint of the design domain, V_{max}. Regarding the contact area, post-processing is also imperative to the design of parts for the build. If support structures are not removed properly, the residue can increase the surface roughness of the part [1,35,46]. For more delicate features such as thin-walled designs, removing excess material from the surface could damage the part [50]. Therefore, the amount of contact area between

the part and the support structure, $A_{max,}$ is associated with the post-processing cost required which will be constrained in this model.

3.4.2. Design Domain and Boundary Conditions Definitions

Before the design optimization process begins, the design domain must be defined and input conditions for the ESL analyses need to be obtained. Prior research has shown that the thermomechanical model of LPBF can be divided into a thermal simulation to predict the temperature distribution and a structural simulation to predict structural properties [82]. Two part-scale models, equivalent flash heating (EFH) [18,30,31,61] and inherent strain method (ISM) [16,18,61,74,78,79,82], are employed in this method to predict the thermal and mechanical properties to save computational time during pre-optimization. As opposed to a computationally expensive exact solution to heat source input that considers scan patterns and other phenomena associated with the melt pool, the EFH method is employed for the layer-by-layer simulation [18,31,51]. Details regarding the equations to solve the two-step procedure of heating and cooling of activated elements to simulate the layer-by-layer AM process can be found in Li *et. al* [31].

To begin the layer-by-layer simulation, as shown in Figure 9(a) the column of height, *d*, contains all active elements whereas the overhang elements of height, *e*, are deactivated. For the first heating cycle, a superlayer of elements composed of multiple actual powder layers is activated with a volumetric heat flux at the surface nodes [31]. To calculate the amount of volumetric heat flux, q", the following equation is applied:

$$q'' = \frac{A_b \cdot P}{d_m \cdot d_s \cdot h}, \tag{20}$$

where A_b is the laser absorptivity, P is the laser power, d_m is the depth of the melt pool, d_s is the spot diameter and h is the hatch space. After heating is applied for a user-defined time, the cooling occurs to simulate the amount of time for the re-coater to apply another layer [30]. The cycle of heating and then cooling continues until all overhang element layers have been activated. The base plate is represented as

the heat sink and is kept at a constant temperature with an applied convection coefficient [31]. Although the material properties are temperature-independent, to account for the heat loss due to convection and radiation, a convection coefficient is applied to the sides of every activated layer [31].

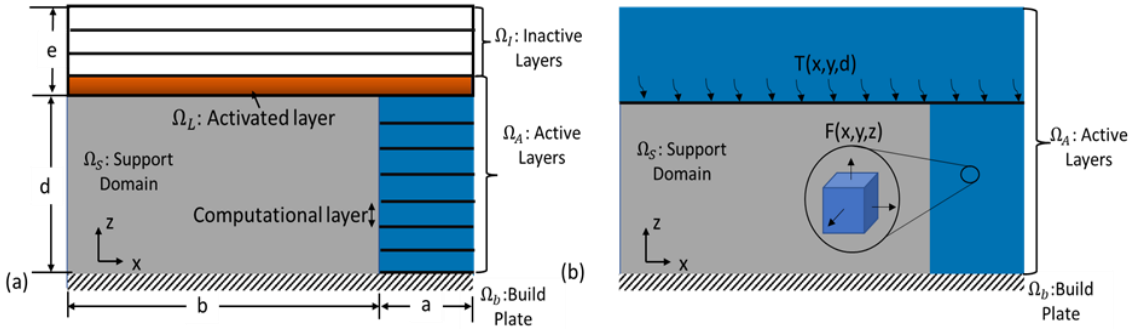

Figure 9 2D schematic of a cantilever beam showing an example of (a) the layer-by-layer process simulation and (b) input parameters for the equivalent steady-state model.

The layers for which the temperature distribution becomes most non-uniform are the locations of the build part that need support structure. The temperature distribution of the non-uniform layer is extracted from the EFH simulation to be used as boundary conditions for the steady-state evaluation, described in Section 3.4.4 and shown in Figure 9(b).

The inherent strain method (ISM) [84] is a popular technique used for AM part-scale modeling to predict residual stress of various geometries, including heat exchanger channels [85,86] and lattice structures [16,87,88]. It is a promising approach for mechanical property prediction due to its efficiency and accuracy for part-scale models, compared to a full thermomechanical analysis [16,74,78,79,82,85]. For this approach, a quasi-static mechanical analysis is performed by applying layer-by-layer activation of an external body force load, obtained from a small-scale thermomechanical analysis, with boundary constraints on each activated element layer, *i* [82]. The governing equation for ISM analysis is:

$$\nabla \cdot \sigma_i = 0, \tag{21}$$

$$\sigma_i = E\varepsilon_e^i, \tag{22}$$

$$\varepsilon_{tot}^i = \varepsilon_e^i + \varepsilon_p^i + \varepsilon_{in}^i, \tag{23}$$

where σ_i denotes the stress field for the *i*-th activated layer and E is the constitutive elastic tensor. The elastic, plastic, inherent, and total strain field for the *i*-th layer are denoted as ε_e^i, ε_{in}^i, and ε_p^i, respectively.

The sequential analysis takes the solution from the previous step as an input boundary condition for the current step.

One major underlying assumption of this model is that the average inherent strain vectors, applied as the coefficient of thermal expansion within the quasi-static structural analysis, are constant [82]. Therefore, applications of ISM on an overhang void of support structure would result in inaccurate results. To address this challenge while still adhering to applied assumptions, a uniformly distributed lattice support structure of the weakest unit cell is placed underneath the overhang. The lattice support structure is assumed to have the same inherent strain vectors as the bulk material [18]. After simulation, the force values only from the part are extracted to be input for the ESL [78], as shown in Figure 9(b).

3.4.3. Definitions of Design Variables

A library composed of pre-defined types of unit cells is utilized as the values of design variables. A large library would enable multiple constraints, such as printability and functionality, to be easily obtainable [57]. However, for this problem, there are m^n possible configurations, where *m* is the number of pre-defined unit cells and *n* is the number of design variables, which increases exponentially with an increased number of unit cells [53]. Therefore, users must define the appropriate unit cells for their optimizers, such as connectivity [57–59]. Commonly reported unit cells found in literature are literature are octahedron [45,58], octet truss [53–56], and body-centered cubic [40,57,60,89]. For this demonstration, three commonly employed strut-based unit cells are selected for their connectivity and manufacturability greater than the minimum strut diameter of 200 microns [56], shown in Figure 4: simple cubic (SC) [4,18,37], body-centered vertical strut cubic (BV) [19], and face-centered cubic (FC) [4,40]. Other types of unit cells also could be included in the library by users when the method introduced in this section is implemented in practice [57]. Each SC, BV, and FC self-supporting cell occupies a 2x2x2 mm^3 space; however, users may define the appropriate cell size when building the library [21,57]. As exemplified in Table 5, each unit cell for AlSi10Mg has properties that are advantageous to the flow of heat (computed using ANSYS Material Designer), the structural integrity, the volume, or the amount of area connected to the part, shown in bold.

For example, SC has a low volume that would attribute to low material cost. BV has a low contact area, resulting in low post-processing costs. Finally, FC has a high thermal conductivity that would decrease the support heat transfer rate into the system.

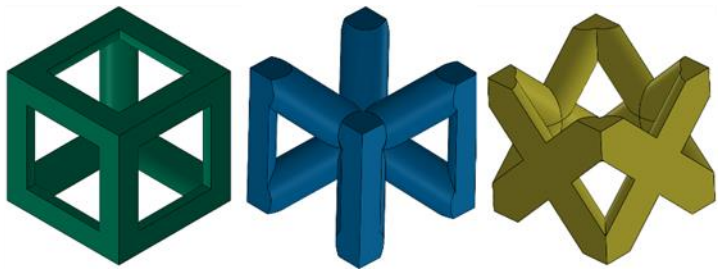

Figure 10 Unit cells employed for lattice support structure heat transfer analysis (from left to right): Simple Cubic (SC), Body-Centered Vertical struts (BV), and Face-Centered Cubic (FC)

Table 5: Physical properties of various unit cells for AlSi10Mg in comparison to an equivalent solid volume. Advantageous qualities in bold.

Unit Cell	$K_{eff}\left[\frac{W}{mC}\right]$	E_{eff_z} $[GPa]$	$E_{eff_{Y,X}}$ $[GPa]$	G_{xy} $[GPa]$	G_{xZ}/G_{yz} $[GPa]$	$Volume$ $[mm^3]$	$Area_{XY}$ $[mm^2]$	$Area_{YZ}$ $[mm^2]$
Solid	110	76	76	27.82	27.82	8	4	4
SC	12.37	7.64	7.64	0.5419	0.5419	1.82	2.31	2.31
BV	24.39	9.73	3.69	4.375	4.175	2.82	0.567	1.30
FC	39.43	19.5	13.4	0.1598	6.873	3.69	0.846	3.24

3.4.4. Sub-Models Evaluations

Running a transient model in each iteration step leads to high computational costs, despite the combination of single-layer activation and superlayers [18,30,61]. Alternatively, ESL models can be performed within each iteration step [30,51]. ESL models require "equivalent" loadings from multi-step models [18,51], therefore, the loadings from the part-scale models run in Section 3.4.2 will be employed as inputs for the equivalent steady-state thermal and ESL structural sub-models. Regarding the thermal sub-model, the temperature distribution from underneath the overhang after applying EFH is inputted as boundaries. This approach is compatible with simple and complex designs [51]; therefore, it will be used

in this study for the evaluation of the minimization of the heat transfer rate through the base plate. In this sub-model, only heat conduction is considered.

The governing equation for this sub-model is

$$q'' = \nabla \cdot (K_{eff} \cdot \nabla T(x)) \tag{24}$$

where q" is the internal heat generated by the system, K_{eff} is the effective thermal conductivity, and ∇T is the temperature gradient [75]. To relate the dissipation of heat to a steady-state model, Fourier's heat conduction law,

$$q' = -K_{eff} dT dz, \tag{25}$$

is evaluated as it relates the rate at which heat flows through any surface per unit area, q', with the conductivity, K_{eff}, the temperature difference between the surfaces for the bottom of the overhang height of z [75]. More specifically, the heat transfer rate, Q_{in}, is calculated by integrating the flux over the area of the element [41,75].

To evaluate the equivalent steady-state mechanical sub-model, the nodal force from the ISM deformed part will be inputted as the applied force for the ESL mesh as an input force. The following governing equation is solved using the FEM solver [76]:

$$\nabla \cdot \sigma = F. \tag{26}$$

In Eq (26), σ denotes the stress field and F is the applied force load vector. The von Mises equivalent stress is utilized for this model to consider the yield criterion. To reduce computational time, the forces from the ISM are extracted from only the part and applied as a load to the optimization model. For each iteration step in the optimization, the p-norm stress and the maximum total displacement are evaluated. If the model exceeds the stress, volume, or area constraints, the design is rejected, and a new design will be searched for.

Given the complexity of the many possible unit cells and configurations within the design domain, a new mesh needs to be generated for each iteration step during optimization. An alternative is to use a simpler representative volume with equivalent material properties, namely, the HA [62]. The basic idea behind the approach is that the effective (i.e., average) properties of RVE can be found by mapping the relationship between the entire domain composed of many RVEs to a single RVE (i.e., a unit cell). This requires solving two physics problems, one at the macroscale and one at the microscale, that are coupled by a scaling factor. More information can be found in a review published by *Hassani and Hinton* [62].

3.4.5. Optimization Process

The modified SA-based optimizer begins with a randomized distribution of unit cells that fill the void design domain at the initial state. The initial state is progressively altered according to the future evaluations of the objective function at a rate defined by the user in the pre-optimization stage, as illustrated in the flowchart in Figure 11. SA is analogous to the annealing of metal from a high-temperature state (i.e., molten) to a low-temperature state (i.e., solid). The starting temperature, T_0, is defined by users to initiate the optimization [48,90]. More information regarding choosing the initial temperature can be found in *Suman and Kumar* [90]. Further temperature reduction can follow the geometric cooling schedule defined as

$$T'_{k+1} = \alpha \times T'_k, \tag{27}$$

where T'_k is the annealing temperature at the *k*-th state (i.e., iteration step), T'_{k+1} is the temperature at the next state, and α is the cooling constant [41,66]. The probability of acceptance is defined as

$$P_{acc} = exp(-(O_{k+1} - O_k)/T'_k), \tag{28}$$

where O_k and O_{k+1} are the energy states (i.e., the values of the objective function) of the previous state and current state, respectively [48,91]. To determine the acceptance of the new proposed configuration, the

computed probability, P_{acc}, is compared to a randomly generated number between 0 and 1. If P_{acc} is greater than the random number, the inferior design state is accepted; otherwise, it is rejected.

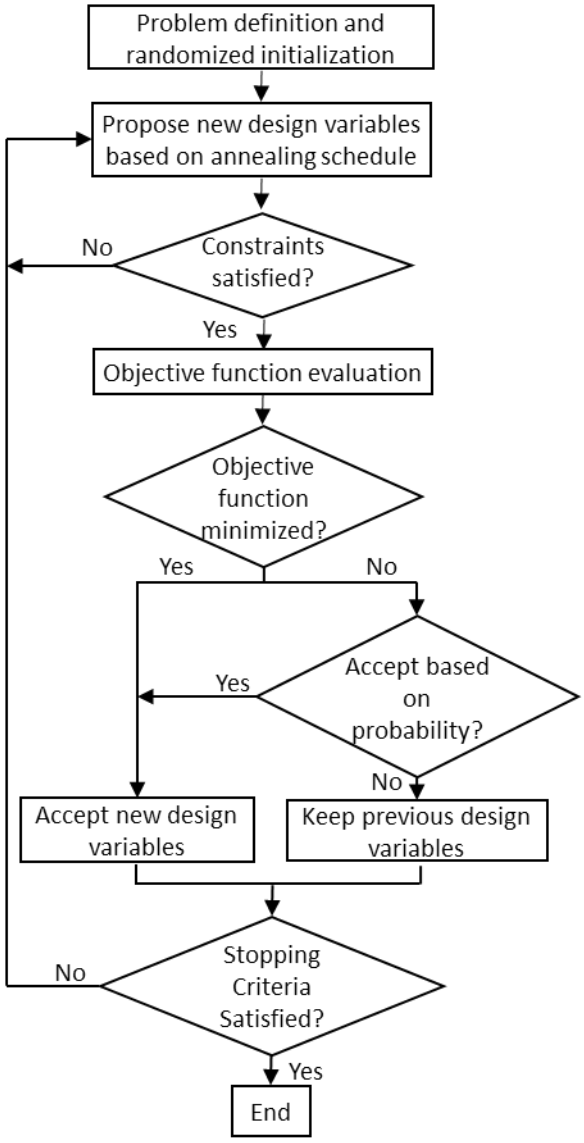

Figure 11 Flowchart of the proposed modified SA-based optimizer of thermally conductive support structure

One limitation of the traditional SA optimizer is the limited number of design variables changed in every iteration step (i.e., small changes in between proposed configurations) before evaluating the objective function [48]. With a large number of design variables for the lattice support structure design, it would be inefficient to optimize by performing only a couple of moves (i.e., swap of the unit cell for another randomly chosen unit cell) per iteration step given that there are m^n possible configurations, where m is the number

of unit cell types in the library and n is the number of design variables. Therefore, to encourage a wider search of the design solutions for practical application, a modification for the traditional SA optimizer method is made to the number of swaps per iteration step, which is now dependent on the annealing schedule.

The proposed optimizer can be described in three stages: exploration, intermediate, and fine-tuning. The exploration stage occurs at high annealing temperatures when there is a high probability of accepting an inferior design. This stage allows an extensive search of the design domain. Given the exponentially declining nature of the geometric annealing schedule, this stage is relatively short compared to the other two stages. Within the intermediate stage, the optimizer performs a more restrictive search within a concentrated region. Finally, the fine-tuning stage occurs at low annealing temperatures and enables the optimizer to locally search the design domain by iterative improvements. The geometric schedule biases this stage until the stopping criteria has been reached. The transition between two stages is determined based on the frequency, P_{acc}, defined in Eq. (28). The iteration threshold value for the exploration stage is defined by the maximum iteration number in which P_{acc} is utilized 50% of the time. For the intermediate stage, the iteration threshold is between the exploration stage threshold and a maximum number of subsequent iterations to reach a frequency of 25% utilization of P_{acc}. The successive iterations are denoted as the fine-tuning stage.

With the baseline of a constant number of swaps for each stage identified, a stage-dependent annealing swapping strategy is introduced to improve the efficiency of the traditional SA optimizer and shown in algorithm 1. This modification correlates the three stages with the number of user-defined swaps per iteration. During the initial stages, a rigorous exploration occurs by setting the number of swaps equivalent to n or *swap_max*. As T'_k decreases, the number of swaps also decreases until the final stages of the design for which the number of swaps is at its lowest per iteration step, *swap_min*. As an example, in the case study demonstrated in Section 3.5.1 with the cantilever beam, there are $n = 225$ design variables and $m = 3$ pre-defined unit cells. There will be 225 randomized swaps that occur during the exploration stage, meaning

225 randomly selected unit cells are exchanged with a pre-defined unit cell before the objective function and constraints are evaluated. Subsequently, the intermediate stage is defined as a constant of 25 swaps per iteration. By the time the fine-tuning stage is reached, there is only one randomly selected unit cell swapped between each iteration until the stopping criteria is reached. The stopping criteria of this optimizer can be when T'_k reaches the minimum temperature [66], the convergence tolerance [67], or a number of iterations [68,69]. Notably, algorithm 1 is programmed in Python using a customized SA algorithm to perform optimization and a commercial FEM solver, ANSYS APDL, is utilized for thermal and structural evaluations using the pyAPDL interface (i.e., *evaluate()* and *evaluate_constraint()*). All evaluations include the automated meshing using SOLID185 elements and material assignment.

Algorithm 1 Modified Shape Annealing Algorithm

```
initialize SA hyperparamters (e.g., T, α)
generate initial_state
state = evaluate(initial_state)                    #Run pyAPDL for static structural analysis
state = evaluate_constraint(initial_state)
    procedure Simulated Anneal(state, T, α, swap_max, swap_inter, swap_min)
        while T > 0.1 do
            prev_state = state
            if T is in the exploration stage then
                swap = swap_max
            else if T is in the intermediate stage then
                swap = swap_inter
            else
                swap = swap_min
            end if
            new_shape = num_swap(swap)
            constraint = evaluate_constraint (new_shape)      #Run pyAPDL for static structural analysis
            if new_shape complies with constraints then
                new_state = evaluate(new_shape)    #Run pyAPDL for steady-state thermal analysis
                test = metropolis(new_state,prev_state,T)
                if test then
                    state = new_state
```

end if

end if

$T'_{k+1} = T'_k * \alpha$

end while

end procedure

3.5. Case Studies

In this section, a cantilever beam and an aerospace bracket are employed as case studies to validate the method introduced in Section 3.3. The material used in this work is AlSi10Mg with a solid Young's Modulus of 76 GPa, yield strength of 314 MPa, and Poisson's ratio of 0.3 [32]. A library composed of three types of unit cells (m = 3), as shown in Figure 10, is utilized to design a lattice support structure able to both dissipate heat and anchor the build part to the build plate. By applying homogenized mechanical and thermal material properties and equivalent steady-state models, the objective function is quickly evaluated. In combination with the stage-dependent annealing swapping strategy to increase design exploration, the optimizer generates lattice support structures that leverage the strengths of each unit cell.

3.5.1. Cantilever Beam

The cantilever beam is a commonly employed benchmark design for the study of support structures [13,15,16,18,30]. Corresponding to the geometric parameters found in Figure 8(a) the dimensions chosen for the cantilever beam are: a = 4 mm, b = 18 mm, c = 10 mm, d = 10 mm, e = 1 mm. By employing m = 3 unit cell types (i.e., SC, BV, and FC) and n = 225 locations for the unit cells, the objective is to find the optimal distribution to minimize the total Q_{in} into the structure Eq. (10), constrained by the weak form of thermal steady state, Eq. (11), and static structural, Eq. (12), governing equations. Stress is considered in this problem using p-Norm stress, Eq. (13). According to NASA, the safety factor for aerospace components is 1.5 [92]; therefore, the maximum stress ratio is set at 0.66 (i.e., 1/1.5). To calculate the p-Norm stress, p = 15. Another AM design constraint that considers both printability and distortion is the maximum sum of deformation, Eq. (14). Given the L = 30 μm and ρ_{shr}= 1 the absolute maximum z-displacement, U_z, is set to 30 μm. The maximum deviation of 1° [83] (i.e. $U_x = U_y$ = 8 μm) is chosen for the top overhang, resulting

in U_{max} = 32 μm. Manufacturing costs are also considered within this problem by constraining volume for material cost, Eq. (15), as V_{max} = 750 mm^3, and contact area for post-processing costs, Eq. (16), as A_{max} = 140 mm^2.

The pre-optimization steps, outlined in Sections 3.4.2 and 3.4.3, are first performed to determine the input values for each sub-model's ESL analyses. Beginning with the thermal analysis, EFH is performed for the same cantilever beam. After each layer is activated utilizing the process parameters (Table 6), the temperature underneath the overhang is extracted from the model after heating, averaged across the length of the overhang, and plotted in Figure 12. The results show that after heating the first superlayer, the temperature along the x-axis exhibits a large jump in temperature from the column directly connected to the base (x < 4 mm) to the overhang (x ≥ 4 mm). This is expected within LPBF as the temperature will be significantly higher above the powder due to the lower thermal conductivity of the powder compared to the bulk material [30,34]. For this study, the temperature distribution across the top of the cantilever for the first layer will be utilized as the applied thermal load for the design domain in the steady-state optimizer evaluation. By inputting the temperature distribution, the temperature along the length of the overhang can ensure the heat flow is not biased to the completely solid column, but through the support domain. The layer-by-layer mechanical analysis is also performed with inherent strain vector inputs from Table 6. After all activations are performed, the forces of only the cantilever beam are extracted as input for the model.

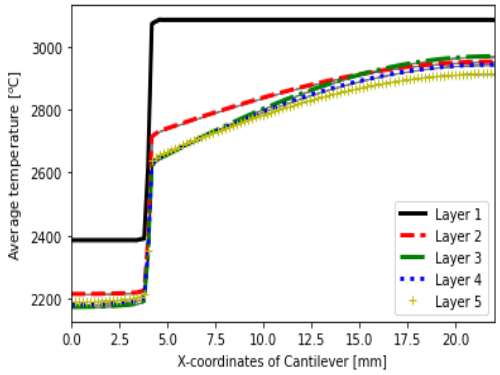

Figure 12: Temperature transition of LPBF process: represents temperature at the end of the heating process for the computational layers extracted from underneath the overhang of the cantilever beam.

Table 6: Parameters for layer-by-layer application [8,11]

Process Parameter	Value
Volume heat flux, q $[W/m^3]$	1.96×10^{13}
Convection Coefficient for heat loss to environment, h_{side} $[W/m^2°C]$	100
Convection Coefficient for heat loss to build plate, h_{plate} $[W/m^2°C]$	8,000
Heating time per layer, t_h[s]	4×10^{-4}
Cooling time per layer, t_c [s]	5
Build plate temperature, T_{amb} [°C]	20
Inherent strain vector in x, y, z	-0.016,-0.016, 0.014

In addition to the inputs from the part-scale models, the user-defined parameters must be inputted. For this case study, the stage-dependent number of swaps begins the exploration stage with a rigorous design exploration of swaps with 225, equal to the number of design variables, n. During the intermediate stage, the number of swaps decreases to n/10 whereas the fine-tuning stage ends with one swap per iteration step. The hyperparameters of the modified SA are chosen as $T_0 = 50$ and $\alpha = 0.5$. For this case study, the stopping criteria is chosen as a minimum T'_k of 0.1, which has been shown in literature to have a high convergence speed [66]. When the stopping criterion has been reached, $T'_k < 0.1$ [66], the results are compared to the four benchmark structures composed of uniformly distributed unit cells (e.g., FC Only).

With the input from the two sub-models obtained and the user-defined parameters, the optimization procedure begins with the randomized material distribution that is initially evaluated then the first iteration step begins. The amount of heat dissipation from the cantilever to the build plate is measured as the minimization of heat transfer rate into the system, Q_{in} through conduction only, which results in a negative value. The HA allows for the representation of a block-like structure (i.e., RVE) that is meshed into 0.5 mm^3 hexahedra. The optimization process is run 30 times to obtain a statistical average and standard

deviations for the traditional SA, using 1 swap per iteration, and the method proposed in Section 3.4.5, incorporating the stage-dependent annealing swapping strategy. The iteration histories for both optimizers are plotted in Figure 13. Using a desktop computer with Intel Core i7-7700 CPU and 32 GB RAM, each run takes approximately 2 hours per simulation resulting in about 3 seconds (s) per iteration step. For the traditional SA optimizer, the linear decline of the objective function indicates a less efficient search within the design domain compared to the proposed method. The results also illustrate the initial design dependency of the traditional SA optimizer due to the larger deviations, represented by the shaded regions, from the average result. Moreover, by running 30 times, the sensitivity of the modified SA-based method to the randomized acceptance, swapping, and initial configuration state can also be evaluated. The sensitivity can be measured through the reliability of the algorithm using the coefficient of variation [93]. For this case study, the coefficient of variation is 1.70% for the cantilever beam, indicating that the method is not sensitive to the randomization of acceptance, swapping, and initial configuration.

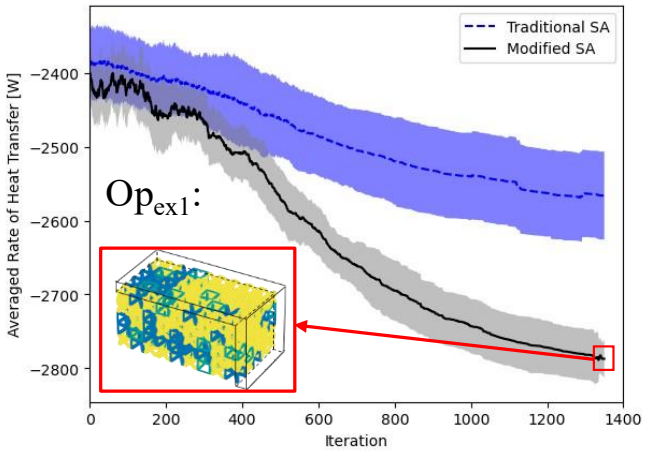

Figure 13: Average objective function values for the heat transfer rate of the traditional SA optimizer and the proposed method for the cantilever beam case study. Shaded regions show standard deviation with an example Op_{ex1}, with final values: Objective = -2,815 W, Volume = 735 mm^3, Area = 108 mm^2, p-Norm = 0.366, U_{sum} = 24.2 mm

Table 7 shows the results from the optimization which compares the average of 30 computationally designed structures, $Op_{avg,1}$, to the uniformly distributed benchmark designs. The results indicate that the computationally designed hybrid support structure with a distributed combination of SC, BV, and FC unit cells satisfies all the constraints defined by Eqs. (13) – (16) and achieves an average ~60% reduction in

material cost and ~62% reduction in post-processing costs compared to a completely solid support structure. The BV Only benchmark design also satisfies the constraints but $Op_{avg,1}$ has an average of 14% better heat dissipation and a 25% reduced deformation than BV Only. Notably, FC is the most favorable unit cell to achieve the highest heat dissipation and stiffest structure, but the support structure uniformly distributed with FC unit cells (FC Only in Table 3) cannot satisfy the inequality constraint for the volume of the support structure, V(x). Furthermore, it should be noted that heat transfer through the solid column is utilized for all configurations (up to height *d*). The exact fraction of flow through the solid domain versus the support structure domain was not computed and would be interesting to include in future work. Given that the non-uniform temperature distribution from the laser is applied at height *d*, the area above the support domain is receiving the most amount of heat as it accounts for 81% of the total area. Thus, it is expected that most of the heat is flowing through the support structure.

Table 7: Comparison of the benchmark results to the average of 30 computationally designed structures for the cantilever beam case study, $Op_{avg,1}$, with standard deviations shown in parentheses for the optimizer.

	$\|Q_{in}\|$	V(x)	A(x)	p-Norm Stress	Max(U_{sum}) [μm]	SC/BV/FC	V(x)<750 A(x)<140 P-norm < 0.66 Max(U_{sum}) < 32
Solid	7,128	1,800	280	0.293	8.06	--	No
SC Only	1,743	409	161	0.359	31.7	225/0/0	No
BV Only	2,405	**634**	**57**	0.365	30.8	0/225/0	Yes
FC Only	3,235	830	120	0.352	15.6	0/0/225	No
$Op_{avg,1}$	**2,773 (47.1)**	722 (11.7)	107 (6.82)	**0.360 (0.00614)**	**24.0 (1.34)**	27/63/133 (5.3/8.0/9.4)	Yes

When comparing the final results of the steady-state thermal model of a result chosen from the 30 computationally designed configurations, Op_{ex1}, using HA to the exact representation, there is a 0.12% error for Q_{in}, indicating a HA is a good approximation method for the exact model. The part-scale models are also performed to validate the use of ESL analyses. For the thermal analysis, the transient thermal model utilizing EFH is performed on the full cantilever model using the Op_{ex1} lattice support structure and compared to the cantilever without support. The maximum temperature on the cantilever beam without supports is 437°C after 5s of cooling; whereas, the maximum temperature of Op_{ex1} is 27°C. This result is

expected, as the heat required to fabricate the overhang dissipates through the lattice support structure without needing excessive material (e.g., solid support structure). Thus, the equivalent steady-state thermal loading applied to the optimizer can be utilized as inputs for an approximation to expedite evaluation. ISM is performed for Op_{ex1} and is compared to the initial case of the SC Only structure to validate the ESL structural analysis utilized for the optimizer. It is expected for the ISM model utilizing Op_{ex1} to outperform the ISM part-scale model utilizing the SC Only structure. When comparing the maximum U_{sum} deformation in the cantilever beam utilizing SC Only to Op_{ex1}, there is a 16% decrease in maximum deformation. These results indicate that utilizing an ESL structural analysis can yield better deformation properties without needing the part-scale simulation between each iteration step.

3.5.2. Aerospace Bracket

AM has been widely adopted within the aerospace industry to fabricate components with complex geometries, yielding about 12% of total AM industrial use [94]. Components designed for the aerospace industry, such as brackets, must be lightweight and achieve a near-net shape. An aerospace bracket inspired by the design of *Xiaohui et al.* [73], shown in Figure 8(b), is chosen for the demonstration of the method proposed in Section 3 as it provides a practical case in which the dimensionality of the problem is high and there are multiple overhangs to consider. Given the two-plane symmetry of the bracket, only a quarter will be simulated, resulting in optimizing the configuration of two overhangs to maximize heat dissipation: long and short. Following the dimensions of Figure 8(b), the long overhang has dimensions: a = 2 mm, b = 8 mm, c_{long} = 48 mm, d = 24 mm, e = 2 mm. The short overhang has the same a, b, d, and e dimensions but the length of the overhang, c_{short}, is set to 26 mm. With the design domain defined, the objective is to find the optimal distribution of m = 3 unit cell types for n = 1,776 locations for the unit cells to minimize the heat transfer rate, Q_{in}, into the structure. The maximum stress is defined as the maximum ratio of the p-Norm stress to the yield stress of the material, Eq. (13). Adhering to the 1.5 safety factor for aerospace components [92], the maximum stress is set to 0.66 with p = 8 [80]. With the maximum deviation of 1° of the overhang for U_x and U_y (i.e. 34 μm) and the relative density ρ_{sh} is set to 0.5 [79], U_{max} = 76 μm for the

displacement constraints, Eq. (14). The volume constraint is set to V_{max} = 5,900 mm^3 and the interfacial area is selected to be A_{max} = 1,360 mm^2.

The pre-optimization stage begins by running the two part-scale models to obtain the ESL for steady-state thermal and static structural sub-models run during the optimization implementing the process parameters from Table 6. EFH is performed for the two overhangs (i.e., long and short) with an average element size, and superlayer thickness, of 1 mm^3 with temperature distribution extracted from the model after heating and plotted in Figure 14. The temperature distribution from superlayer two from the two overhangs is used as input for the steady-state thermal analysis. The default support structure utilized for the ISM layer activation is a uniform distribution of SC with homogenized properties. The forces of both overhang structures are extracted as ESL for the support structure design problem.

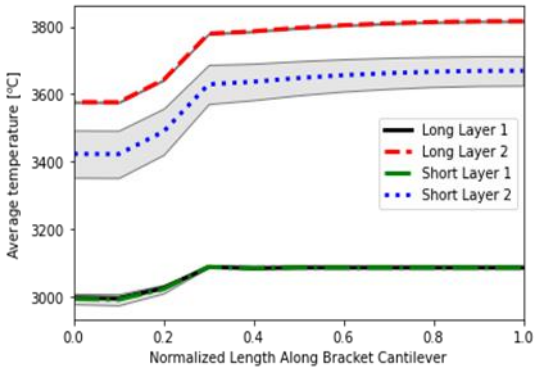

Figure 14: Temperature transition of LPBF process: represents temperature at the end of the heating process for the computational layers extracted from underneath overhang of aerospace bracket with standard deviation represented by the shaded region.

For this case study, the stage-dependent annealing swapping strategy begins with an extensive search of the design domain within the exploration stage consisting of 1,776 swaps, also equal to the number of design variables, n. During the intermediate stage, the number of swaps decreases to $n/10$ and is finally set to $n/100$ during the fine-tuning stage. Utilizing the inputs from the sub-models, the hyperparameters are set to $T_0 = 50$ and $\alpha = 0.5$ and optimization begins. For this demonstration, the stopping criteria is chosen as a set number of iterations, to consider the pragmatic termination associated with the computational time of 12-hour runs, which allows the method adequate time to demonstrate its effectiveness. When the stopping criteria of 1,400 iterations have been reached, taking approximately 3 seconds per evaluation time, the

results are compiled and compared to the benchmark designs of uniform lattices. Notably, the computational time is predominantly due to the amount of time to assign the material properties (~45 seconds) using pyANSYS. Future work should consider expediting the material assignment for high-dimensional problems.

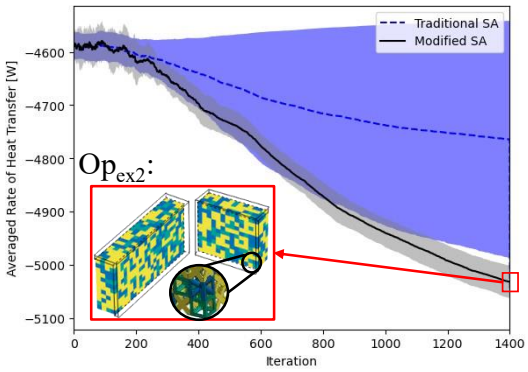

Figure 15: Average objective function values for the heat transfer rate of the traditional SA optimizer and the proposed method for the aerospace bracket case study. Shaded regions show standard deviation with an example Op_{ex2}, with final values: Objective = -5,039 W, Volume = 5,481 mm^3, Area = 1,243 mm^2, p-Norm = 0.648, U_{sum} = 69.7 mm.

The iteration histories of 30 averaged computationally designed structures for a traditional SA optimizer of a constant 17 swaps per iteration (i.e., about 1% of the total number of design variables) and the proposed method with the stage-dependent annealing swapping strategy are plotted in Figure 15. Although the heat transfer rate into the system decreases for both optimizers, the traditional SA optimizer has a larger deviation. This is because the traditional SA optimizer is heavily reliant on the initial state and is unable to make enough changes to effectively improve the objective function. Further evaluation is performed to compare the average computationally designed results, $Op_{avg,2}$, to benchmark designs, shown in Table 8. By running multiple times, the sensitivity of the method to the randomized swapping, acceptance, and initial configuration state is captured [93]. The coefficient of variation is used to describe the sensitivity of the 30 runs, which is 0.63% for the aerospace bracket. When comparing the uniformly distributed structures to $Op_{avg,2}$, it is the only set of structures that satisfies all the constraints. The material cost, represented by the volume of the support structure, $V(x)$, is one of the major contributors to the overall expense of printing a part using AM [51,59]. The cost estimation of using a completely solid support

structure compared to $Op_{avg,2}$ results in savings up to 61%. Post-processing cost, yielding about 8% of manufacturing cost [9], is directly proportional to the amount of time to post-process [59], which varies based on the process and machinist [26]. Assuming increased contact area scales linearly with increased post-processing time, it would cost 47% less to post-process the $Op_{avg,2}$ compared to the solid. Furthermore, given that heat transfer through the solid column is utilized for all configurations (up to height *d*), an exact fraction of flow through the solid domain versus the support structure domain was not computed. However, it is expected that with the applied non-uniform temperature distribution, with 80% of the area belonging to both support structure domains, most of the heat is flowing through the support structure.

Table 8: Comparison of the benchmark results to the average of 30 computationally designed structures for the aerospace bracket case study, $Op_{avg,2}$, with standard deviations shown in parentheses for the optimizer.

	$\|Q_{in}\|$	V(x)	A(x)	p-Norm Stress	Max(U_{sum}) [μm]	SC/BV/FC	V(x) < 5,900 A(x) < 1,360 P-norm < 0.66 Max(U_{sum})< 76
Solid	12,479	14,208	2,368	0.609	14	--	No
SC Only	3,524	3,232	1,367	0.648	96.0	1,776/0/0	No
BV Only	4,624	5,008	661	0.648	97.5	0/1,776/0	No
FC Only	6,004	6,553	1,568	0.637	74.7	0/0/1,776	No
$Op_{avg,2}$	**5,041 (31.9)**	**5,505 (19.6)**	**1,247 (18.0)**	**0.642 (0.0053)**	**68.8 (4.6)**	301/557/918 (11/18/17)	**Yes**

A lattice support structure selected from the 30 computationally designed structures is used for validation, Op_{ex2}. When comparing the homogenized representation to the exact representation of the unit cells for the equivalent steady-state model, the error in Q_{in} is 0.337%. To address the approximation of equivalent steady-state, the part-scale model of EFH is run. Without supports, the maximum temperature after 5s of cooling is 857°C for the long bracket's second applied layer and 721°C for the short bracket's second applied layer. These temperatures are well above the melting temperature of AlSi10Mg, 600°C [31], which indicates that there is a high probability of part deformation and machine damage. In contrast, Op_{ex2} has a maximum temperature of 225°C for the long bracket's second applied layer and 183°C for the short bracket's second applied layer. ISM is performed for a quasi-static analysis on Op_{ex2} to validate the use of

the ESL input force loading. Compared to the SC Only structure employed as the benchmark, a 12% decrease in max U_{sum} is achieved. This reduction in maximum deformation validates that a part scale model, which could result in minutes or hours per iteration depending on the model, can be approximated using ESL, which takes 3s per iteration. By utilizing a hybrid lattice support structure, the manufacturing costs were reduced without compromising computational time to run part-scale models.

3.6. Conclusion

A modified SA-based method is introduced to design lattice support structures for LPBF. The novelty of this method is the proposed stage-dependent annealing swapping strategy for efficient design domain exploration and the implementation of homogenization approximation (HA) and equivalent static loading in the design optimization process to save computational costs at each iteration step. The method is programmed using Python, for which commercial software is utilized to mesh and evaluate the simulation-informed objectives and constraints. In addition, ANSYS Material Designer was used to compute the homogenized material properties of the unit cells. The proposed method is applied to two case studies, a cantilever beam and an aerospace bracket, and computationally validated. Results show that the optimal hybrid lattice structures generated from the method can maximize heat dissipation while saving greater than 60% in material cost and 62% in post-processing costs.

The method outlined in this chapter broadens the application of stochastic non-gradient-based optimizers within the interdisciplinary topic of AM. By distributing self-supporting unit cells with known material properties with this method, multiple optimal lattice support structures are obtained while considering practical material and post-processing costs. Based on the discrete problem formulation, direct comparison to gradient-based optimizers would be infeasible. However, some comparisons can be made regarding the advantages of utilizing a non-gradient-based optimizer such as simulated annealing. One of which is that the approach does not require additional computations of the sensitivity analysis used for traditional gradient-based optimization methods such as SIMP and level-set methods [90,96], reducing the level of complexity of solving the problem for designers. The strategy provides a systematic approach to

further explore the design domain while circumventing time-consuming evaluations of the simulation-based objective functions and constraints.

4. Chapter 4: A Multi-sized Voxelization Approach to Design Lattice Support Structures for Complex Geometries

4.1. Overview:

Composed of individual unit cells strategically arranged to achieve a desired function, lattices are a promising solution for LPBF support structure design. Despite their many advantages (e.g., multifunctionality and reduced manufacturing cost), remaining challenges prevent their widespread adoption. One of the existing challenges is its difficulty to design for complex structures, attributed to the high computational cost for design exploration and iterative evaluation. Although Chapters 2 and 3 have shown that a modified-simulated annealing method (M-SA) can reduce these computational costs, it has only been applied to horizontal support domains. Thus, this work introduces a novel multi-sized unit cell approach to designing lattice support structures for structures with curved surfaces. Assuming a solid transition region between part and support structure, the library of pre-defined unit cells is expanded to demonstrate the use of multi-sized cells to reduce material waste. The voxelized shape approximation is also implemented to reduce computational cost and error associated with non-uniform meshing. Coupled with M-SA, the approach is validated through the case study of a super-critical carbon dioxide heat exchanger adapter pipe with two unit cell sizes. The computationally designed results are compared to benchmark designs of uniformly distributed single-unit cells. With AM constraints satisfied, the M-SA achieves an average heat dissipation that is 16% higher than the uniformly distributed benchmark of simple-cubic 2-mm unit cells and 19% lower maximum deformation in z within 800 iterations.

4.2. Introduction:

Laser powder bed fusion (LPBF) enables the fabrication of complex metal geometries with features unattainable by traditional manufacturing approaches [1]. For parts with features, such as overhangs, support structures are imperative for the success of their build due to their thermomechanical properties. Lattice structures are a promising approach to generate these supports as they have many attractive qualities that are beneficial for support structures [7,8]. The design of each unit cell within the lattice allows for

tailorable properties (e.g., thermal and structural), lightweight design, and suitability of powder removal. To generate support structures that dissipate heat and anchor the part down to the build plate, optimization methods have been employed to design lattice support structures with reduced manufacturing costs. Due to the typical, box-like structure of the unit cells, much effort has been demonstrated in optimization techniques for horizontal surfaces (e.g., cantilever beam [13,15,18,74]), dismissing the major advantage of complex design granted by LPBF.

Optimization approaches are needed for the design of support structures for functionality and manufacturing cost reduction, especially for costs associated with the material. Some researchers have presented approaches for lattice support structure design for complex structures [7,8]. The difficulty in designing these structures for curved and inclined surfaces is attributed to the connection of the box-like unit cells. The intricate shape of the surface can result in non-uniform connection volume, rendering it difficult to predict the properties of such irregular connections [21,23]. Solid connections can be utilized but may drive up manufacturing costs (e.g., material cost and post-processing costs). To reduce these costs, researchers have explored approaches such as using non-solid (e.g., thin walls or points) [23,25,26] or solid pin connections [13,19,21]. Despite the weight reduction abilities, current approaches can still result in part deformation [17,21,23,26] or high computational cost to explore the design domain [17,19,21], especially when considering individual pin connections. Alternatively, pre-defined unit cells with predictable properties can be employed to reduce computational costs. This approach was recently employed with a new optimization method based on the traditional simulated annealing (SA) optimizer, introduced in Chapters 2 and 3. With the aim to aid designers in the design of lattice structures made by LPBF, this modified simulated annealing-based method (M-SA) was demonstrated to efficiently explore the design domain through reduced iteration count and time per iteration compared to the traditional SA. However, this method has only been applied to horizontal surfaces.

Limitations of existing approaches to generate lattice support structures for complex structures through optimization have motivated the proposed multi-sized unit cell approach based on the popular voxel-

modeling technique. The approach utilizes a voxel model to identify and sort the locations of pre-defined unit cells to reduce material costs. Then M-SA is employed to optimize the configuration of the unit cells with its expanded library composed of multi-sized unit cells. To this end, the expanded library and voxelization approach would enable designers to reduce the material cost within the solid connection between the part and the whole unit cells to create printable structures.

The following sections of this chapter outline the proposed approach. Beginning with an expanded background on existing methods, Section 4.3 discusses the current progress and challenges. Section 4.4 introduces the methodology of the multi-sized unit cell approach for the design of lattice support structure for LPBF. The approach is then demonstrated in the case study of a super-critical carbon-dioxide heat exchanger adapter in Section 4.5. Finally, Section 4.6 provides a brief conclusion.

4.3. Background

Lattice structures have been proven as efficient support structures as they are designable for both the thermal and structural functionality of support structures while reducing costs and adhering to AM design constraints [7,8]. By incorporating lattice support structures within the entire build domain, two domains are defined: part and support. The part subdomain, shown in Figure 16, is the desired structure, which is assumed to have a fixed geometry and orientation. This portion carries the most amount of residual stress from the rapid thermal cycle and concurrent melting of multiple layers [23]. To support the part, the support domain is composed of both a bulk support subdomain (BSS) and a transition support subdomain (TSS). The BSS is the largest of the support subdomains and consists of full-sized unit cells. The physical properties of this domain can be obtained using approximation techniques such as homogenization approximation (HA)[16,43,88]. The last subdomain used to connect the bulk support domain to the part domain is the TSS. This subdomain is important as the heat must efficiently transfer from the part to the support without causing heat accumulation and be able to anchor the part to the bulk support domain [23,26]. Given its irregular support volume, it is difficult to predict the properties within this subdomain for

complex surfaces (e.g., curved and inclined) [17,21–23]. Previous research has addressed this issue, but challenges remain. Thus, the current research and shortcomings are described in this section.

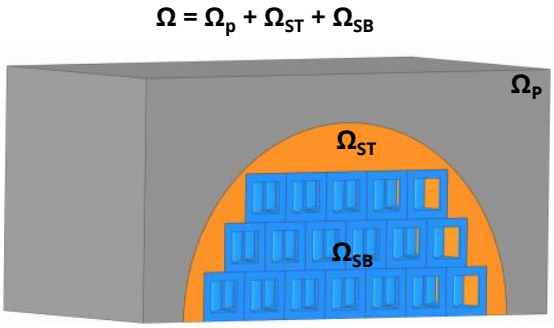

Figure 16: Example schematic of the build domain (Ω) composed of the part (Ω_P), TSS (Ω_{ST}), BSS (Ω_{SB}).

When designing for the TSS, two popular support design approaches are to utilize either non-solid (e.g., thin walls or points) [23,25,26] or solid pin connections [13,19,21,26]. Both connections are favored over purely solid connections as they reduce material and post-processing costs. The default for many support-generating commercial software, such as Materialise Magics® [26,97], is the creation of non-solid structures connected by thin walls or points. One of the most common is the block structure, a lattice support structure composed of periodically repeated thin-walled unit cells [23,25–27]. Although users can adjust the size of the unit cells, the drastic change in surface area between the part and lattice make it the weakest connection [23,24]. This is particularly apparent in overhang features with large surface areas or tall structures, causing build failure or machine damage [16,23,27,73]. In addition, shrinking the unit cell size makes it difficult for trapped powder to leave, thereby increasing material costs.

Alternatively, pin connections can be employed. The popularity of this connection is attributed to its geometric simplicity and design for functionality (e.g., dissipate heat [13,26] and structural integrity [19,26]). Combining pins with a lattice structure design within the bulk support subdomain reduces material waste and can allow for connection to complex geometries [13,19,21]. Optimization techniques must take careful consideration of the pin distribution and sizing to ensure both pin printability [21] and connection functionality [28]. One example of utilizing fixed-thickness pin joints for complex geometries is presented

in combination with multi-sized cells. A computationally designed lattice support structure is generated within a two-step approach for a skateboard bracket to minimize structural compliance constrained by volume. By employing three-unit cell sizes to computationally design the configuration, up to 42% reduction in support volume was achieved. However, this approach was shown to only undergo a single iteration, potentially due to the computational cost of running simulation-informed evaluations at each iteration. The lack of iterative design optimization caused the build failure of the bracket through the failure of the pin connections. To circumvent problems due to pin connection printability, researchers have shown the potential of utilizing teeth [22,27] or self-supporting unit cells with parametric struts [19]. This allows for more control over the strut properties and distribution, especially with the additional pruning step applied at the end. The approach was applied to design lattice support structures with minimized volume that sustains the overhangs for a curved surface. A major shortcoming to this approach is the practicality when incorporating simulation-informed results. The computational cost would drastically increase when many struts are needed to anchor the part and dissipate large amounts of heat from the overhang to the build plate.

Chapters 2 and 3 have shown that a modified-simulated annealing-based method (M-SA) can be employed to generate lattice support structures that are designed for the multi-physics requirements of support structures (i.e., thermal dissipation and structural integrity) with reduced computational cost. By incorporating stage-dependent annealing swapping, the M-SA reduces the number of iterations needed to explore the design domain. Furthermore, by including equivalent static loading (ESL) and homogenization approximation (HA), the computational cost of evaluating simulation-based equations in each iteration is also reduced. However, this method has only been applied to horizontal surfaces. Further modifications to the current modified approach are needed to exploit the capabilities of this method for practical AM parts with complex surfaces.

Despite the extensive study for lattice support structure design, many works neglect the transition subdomain by demonstrating designs for horizontal support domains, such as the cantilever beam

[22,73,74]. Current efforts attempt to broaden the application of lattice support structure design to complex structures by utilizing non-solid or pin connections to reduce volume costs within the transition subdomain. Unfortunately, the efforts have not provided an efficient solution that explores the design domain while considering other AM constraints without increasing the computational cost [19,21]. A promising approach is to employ M-SA to reduce the computational cost, which has been applied to design lattice support structures for horizontal surfaces (e.g., cantilever beams). However, modifications will be needed to consider the material waste within the transition support subdomain.

4.4. Methodology

The research gap defined in Section 4.3 outlines the need for an iterative optimization approach to design lattice support structures for complex structures with reasonable computational costs. M-SA has been demonstrated to reduce the computational cost associated with high iteration count and high computation for simulation-informed evaluations per iteration. Thus, improvements to the M-SA are presented to broaden the application to complex structures by incorporating multi-sized unit cells to reduce material waste within the transition support subdomain. Figure 17 shows the modified flow chart of the M-SA with an expanded unit cell library and additional pre-optimization step of voxelization. Following the outlined method, an overview of the problem is first presented to define the model with the part geometry, pre-defined library, and pre-defined support domain. The two-part pre-optimization step is then executed to identify the bulk support subdomain with corresponding unit cell locations and obtain the equivalent static loadings (ESL) from the two part-scale submodels. Finally, optimization of the unit cell configuration is performed with the objective of maximizing the dissipation of heat (i.e., diffusion of heat flow) while considering AM constraints.

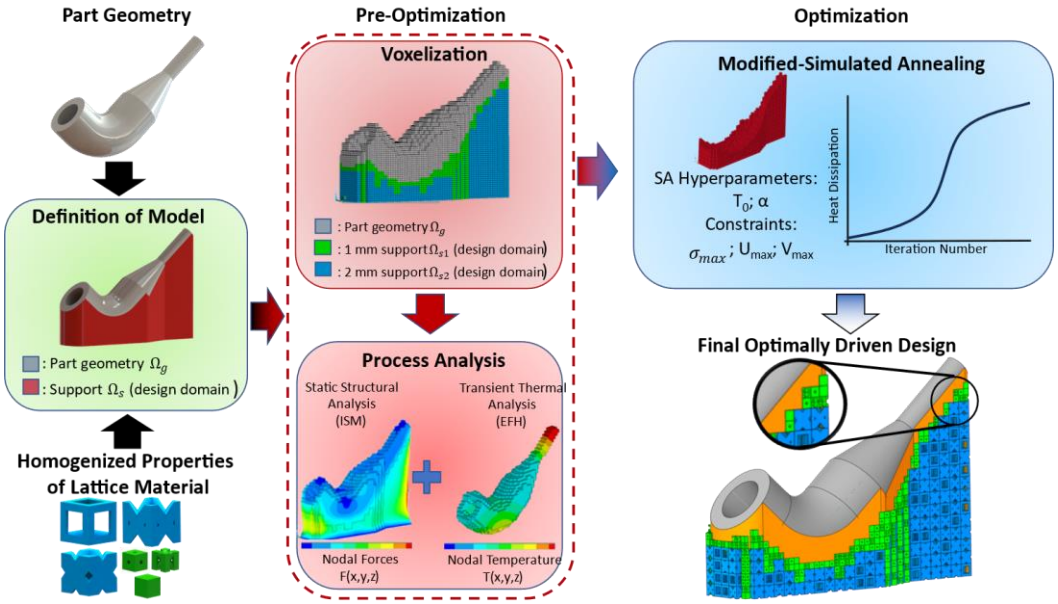

Figure 17: Modified SA-based method flowchart for curved structure

4.4.1. Problem Overview

M-SA has been previously demonstrated to design lattice support structures for LPBF with the objective to maximize heat dissipation while adhering to structural and manufacturing constraints. Modifications have been made to the existing method to expand its application to complex structures and this is demonstrated through the case study of a heat exchanger adapter, shown in Figure 18. As illustrated in Figure 18(b), the adapters are printable when utilizing solid support structures. However, print failure occurs when employing built-in, line support structure designs that have non-solid connections, as shown in Figure 18(c). This build failure is likely a cause of insufficient dissipation of heat which leads to increased thermal distortions, such as warpage. Therefore, the application of the M-SA improved for complex support structures would provide an alternative approach to designing adequate support structures without the expensive trial and error of applying various commercial support structures.

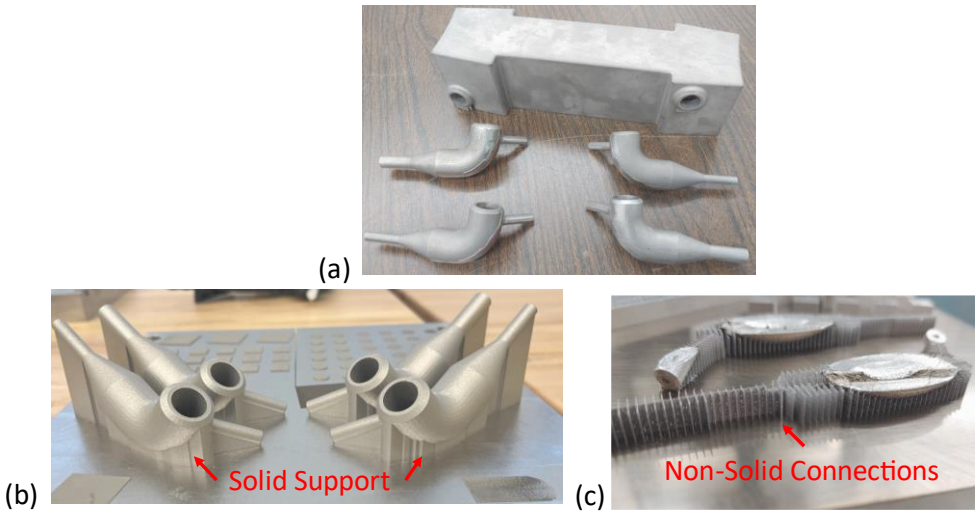

Figure 18: Images of (a) a supercritical carbon dioxide heat exchanger (top) and four adapters (bottom); (b) successful prints of completely solid support structures; (c) failed prints of adapters using default line support structure with non-solid connection.

To adapt lattice support structures for complex geometries (e.g., structures with curved and inclined surfaces) such as the heat exchanger adapter, improvements to the existing M-SA are made. One improvement is the expansion of the library to include multi-sized unit cells, to reduce the volume of the transition support subdomain. Therefore, the problem is reformulated as:

$$\text{Find} \quad f(x,y) = ([x_1,x_2,\ldots,x_m] \text{ and } [y_1,y_2,\ldots,y_k]) \text{ to}$$

$$\text{minimize} \quad Q_{in} = Q(x,y), \tag{29}$$

$$\text{subject to} \quad KT = q, \tag{30}$$

$$CU = F, \tag{31}$$

$$\frac{\sigma_j^{PN}}{\sigma_y} \leq \sigma_{max}, \tag{32}$$

$$U_{sum} \leq U_{max}, \text{ and} \tag{33}$$

$$V(x) < V_{max}. \tag{34}$$

where the design variables, x_i and y_k, are one of the 2 mm and 1 mm pre-defined unit cell types, respectively. There are $i \in \{1, 2, \ldots, m\}$ and $k \in \{1, 2, \ldots, n\}$, possible locations for the 2-mm and 1-mm unit cells, respectively. The design domain is discretized such that the 1 mm unit cells can only occupy where the 2 mm unit cell cannot, as described in Section 4.4.2. The structural constraints that consider the printability

of the part are the maximum p-Norm stress constraint (σ_{max}) and maximum deformation in the *z*-direction (U_z). The p-norm stress is computed by averaging and penalizing *j* clusters of the von Mises nodal stresses and normalizing them using the yield stress of the material (σ_y). Printability is also considered through deformation in the *z*-direction to ensure no recoater blade collision. Finally, the volume constraint employed considers the manufacturing cost as it is directly proportional to the material cost. It should be noted that the contact area is disregarded in this problem formulation as the transition subdomain consists of solid material for maximum connection to the part for heat transfer and structural integrity. However, designers may include additional design variables for the transition domain, such as pins, in future applications.

4.4.2. Design Domain and Boundary Condition Definitions

Voxelization allows for the conversion of any complex geometry into a simplified approximation with cubic structures. It reduces computational costs and errors for difficult simulations, making it a popular approach for geometry representation for AM prediction models [3,5,16,21]. A voxel model is also convenient for the design of lattice support structures as each voxel can represent the location of a portion or whole unit cell [3,16]. As seen in algorithm 2, the approach begins with the input of an STL of the component and pre-defined support domain (*part_support.stl*), the combined model is meshed using MatLab Voxelization Code [98] with corresponding voxel vertices. The vertices are extracted and utilized to create a point cloud, represented by single term voxel_mesh. The STL of only the part (*part.stl*), void of support structure, is then overlayed to identify and remove the points in the point cloud that represent the part using MatLab built-in function in_polyhedron [58,99]. This action is imperative to establish the potential support structure coordinates. Next, the algorithm iteratively finds the locations for full-size unit cells and then sorts and stores the coordinates based on the maximum unit cell size that can hold a complete set of vertices. All points that do not fit the user-defined unit cell sizes can be stored separately for further analysis, such as to represent the transition subdomain. For example, Figure 19(a) shows an example of a symmetrical pipe with its pre-defined support structure representation. The inputted file is then voxelized

and a point cloud of the support domain is created to identify the locations of two-unit cell sizes, Figure 19(b). Coupled with the library of pre-defined unit cells, the number of potential locations defines the total number of design variables. After the locations are identified, the voxel model is meshed (Figure 19(c)) and ready for the part-scale modeling step. Notably, algorithm 2 is programmed in MatLab using a customized algorithm to identify and sort multi-sized unit cell locations. The built-in Matlab functions, mesh_voxelisation [98] and in_polyhedron [99] employed to aid in the approach and can be exchanged for other methods to generate voxel meshes and location of the part.

Algorithm 2 Voxelization

```
voxel_mesh = mesh_voxelisation(part_support.stl)        #[98]
part_vertices = in_polyhedron(voxel_mesh, part.stl)     #[99]
if not part_vertices then
    support_vertices = append ([x,y,z])
end if
    procedure Sort(support_vertices)
        while z_c < z_max do   #current z coordinate less than maximum z coordinate
            while y_c < y_max do
                while x_c < x_max do
                    Central_Vertex = [x,y,z]
                    if all vertices corresponding to Central_Vertex within size 2 do
                        Size_2 = append ([x,y,z])
                    else if all vertices within size 1 do
                        Size_1 = append ([x,y,z])
                    else
                        move to the next vertex
                    end if
                end while
            end while
        end while
    end procedure
```

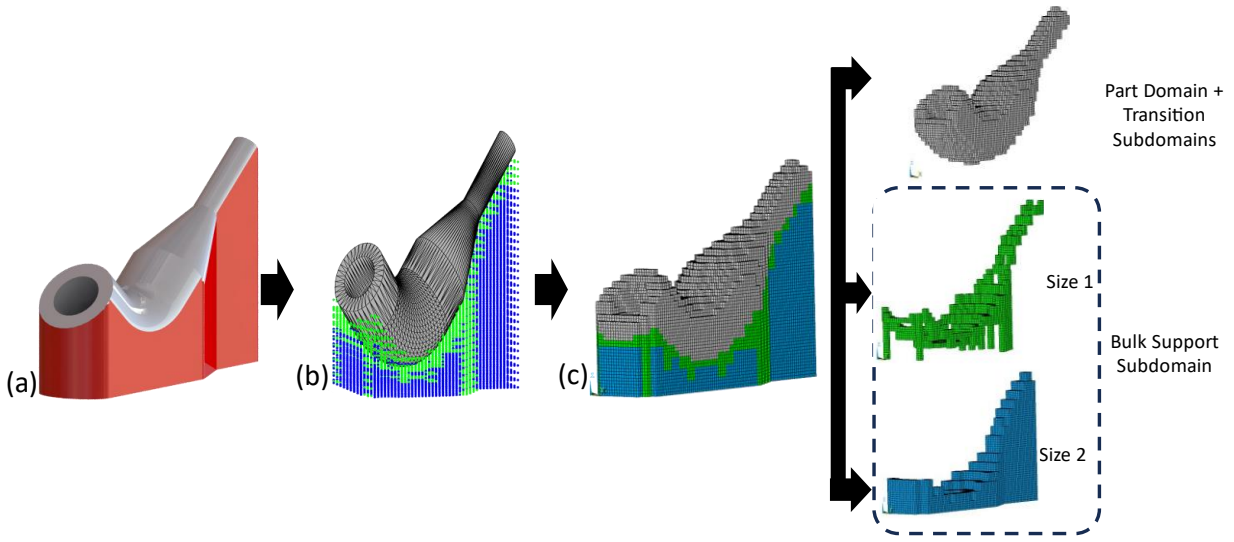

Figure 19: Voxel-based representation for an example part. (a) Exact representation of part with pre-defined design domain, (b) point cloud of sorted voxel vertices, (c) voxel-based mesh representation of part with pre-defined design domain with multi-sized representation.

M-SA employs two part-scale models, equivalent flash heating (EFH) and inherent strain method (ISM), to predict the thermal and mechanical properties of the build with no or poor unit cells, as introduced in Chapters 2 and 3. The voxel mesh is utilized for the part-scale model evaluations as the layer-by-layer loading reduces meshing errors and computational costs [16,100]. For EFH, the part and transition subdomain are utilized, void of support material, to obtain the temperature distribution. ISM is applied to the entire domain, composed of SC for the 2-mm locations and bc for the 1-mm locations. ESL from each model is extracted and inputted into the steady-state thermal and static structural models to be evaluated during optimization.

4.4.3. Design variables

The voxel size resolution is a user-defined feature that depends on the minimum unit cell size set when creating the library during the model definition stage. By increasing the unit cell size selection, designers can achieve more control over the design of the bulk support subdomain. For example, larger cells are useful when reducing the material cost and the build time of the support structure [21,62]. In contrast, small cells are advantageous when increasing the material properties, such as stiffness, and reducing the amount of transition subdomain material. To illustrate the use of multi-sized unit cells, Figure 20 shows examples

of two potential unit cell sizes, 2 mm and 1 mm. Since HA is the approximation technique utilized by M-SA to expedite the evaluation of the static-structural and steady-state thermal submodel analyses, the effective material properties of the unit cells made of nickel-based superalloy, Haynes 282, are computed using ANSYS Material Designer and shown in Table 9.

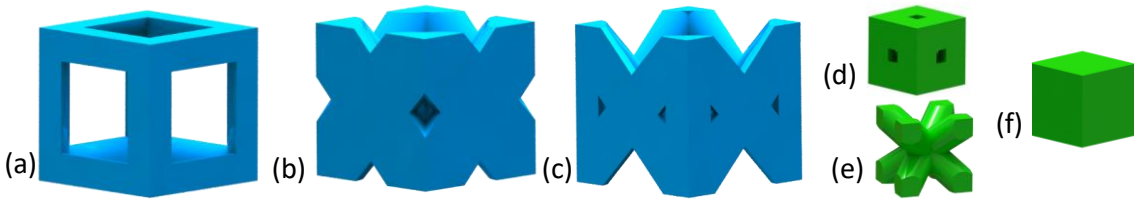

Figure 20: Unit cells employed for lattice support structure heat transfer analysis with (a-c) 2-mm sizes of Simple Cubic (SC), Face-Centered Cubic (FC) and Transition Cell (TR) and (d-f) 1-mm sizes of Simple Cubic (sc), Body-Centered Cubic (bc) and solid (sol).

Proper selection of unit cells and their distribution determine the functionality of the lattice. Each unit cell has different physical properties advantageous to the problem and designed for printability. To generate a library of strut-based unit cells, serval works have proposed methods from varying the density [57] to optimizing the topology [53,100] to interpolating geometries [58] of a few primitive designs. Examples of these primitive designs are typically, octet-truss [53–56], body-centered cubic [40,57,60,89], and octahedron [45,58], which can lead to libraries with hundreds of unit cells [57]. However, incorporating all the potential unit cells would increase the design space exponentially due to the exponential increase in the number of possible configurations [53]. Therefore, researchers have created rules for choosing the unit cells within the library alongside the material properties, such as manufacturability [55,57] and connectivity [57–59]. The unit cell library chosen in this demonstration was selected to enable manufacturability on a Trumpf 3000 printer (i.e., a minimum strut diameter size of 400 microns) and have topological connectivity within their respective sizes.

Consider the 2 mm unit cell, simple cubic (SC) [4,18,37,38], and face-centered cubic (FC) [4,40]. Both are commonly used unit cell designs with contrasting properties for which SC, Figure 20(a), has a low volume but inferior material properties to FC, Figure 20(b). The third 2 mm unit cell is designed to reduce intracellular stress by increasing geometric compatibility for printability, called transition cell (TR), and

possesses intermediate properties between the SC and FC, Figure 20(c). The 1 mm unit cells consist of a smaller simple cubic (sc), a body-centered cubic (bc) [4,40,60,89], and a completely solid unit cell (sol). At a more compact size, sc has superior properties to bc and less volume than sol. The major advantage of using bc is attributed to its low-volume design, providing the optimizer with an option to reduce the volume of a solid unit cell, sol, by half. When utilized in additional applications, other pre-defined unit cells can be incorporated into the library with other properties.

Table 9: Physical properties of various unit cells made with Haynes 282. Advantageous properties in bold.

Size	*Unit Cell*	$K_{effx,y}\left[\frac{W}{mC}\right]$	$K_{eff,z}\left[\frac{W}{mC}\right]$	E_{eff_z} $[GPa]$	$E_{eff_{Y,X}}$ $[GPa]$	G_{xy} $[GPa]$	G_{xZ}/G_{yz} $[GPa]$	$Volume$ $[mm^3]$
	SC	1.54	1.54	30.8	30.8	2.92	2.92	1.82
2mm	TR	1.91	2.96	31.3	51.9	2.07	1.39	3.02
	FC	4.331	5.58	79.5	104	14.6	32.6	3.69
	sc	6.84	6.84	135	135	44.8	44.8	0.7839
1 mm	bc	3.79	3.79	39.4	39.4	26.7	26.7	0.5571
	sol	10.30	10.30	217	217	82.2	82.2	1

4.4.4. Optimization

Simulated annealing is a non-gradient-based optimization technique that finds design solutions by imitating heuristics from the annealing of metal [48]. For which, the optimizer begins with a user-defined initial optimizer temperature, T_0, and an initial energy state (i.e., objective function), O_k. As the temperature of the optimizer cools according to an annealing temperature, the optimizer explores the design domain to minimize (or maximize) the energy state in search of the global optimum. The optimizer temperature-dependent search of the design domain can be divided into three stages: exploration, intermediate, and fine-tuning. Each of these stages can be described by the probability of accepting an inferior design, P_{acc} [48,91]. During the exploration stage, the probability of accepting an inferior design is high, enabling a wide search. As the temperature, T_k, is reduced, P_{acc} is also reduced, which allows a more localized search. For the traditional SA, this could take many iterations and model tuning to reach a reasonable solution given the

small perturbations (e.g., swapping of unit cells) made to the configuration per iteration, particularly for high dimensional problems. However, M-SA exploits the defined three stages to broaden the design domain search by incorporating a stage-dependent annealing swapping strategy for lattice support structure design. During the exploration stage, there is a high number (e.g., equivalent to the number of design variables) of unit cell swapping. When the optimizer transitions to the intermediate stage, the number of swaps decreases as well. Finally, during the fine-tuning stage, the minimum number of swapping is made to the design. More detailed information about M-SA optimization can be found in Chapters 2 and 3.

4.5. Case Study

Supercritical carbon dioxide heat exchangers (sCO_2 HX) are commonly used in nuclear reactors and steam plants [101]. Known for their high efficiency in cooling systems, they have recently been shown to have great potential in the nuclear and solar energy fields [102,103]. To test the efficiency of the heat exchangers, an adapter, shown in Figure 21(a), has been designed to connect both sides of the heat exchanger. Given the need for strong resistance to corrosion and creep [101,103], the adapter used in this study is made from Haynes 282, a nickel-based superalloy. In addition to the material properties shown in Table 9, this material has a Young's Modulus of 217 GPa, yield strength of 715 MPa, and Poisson's ratio of 0.319.

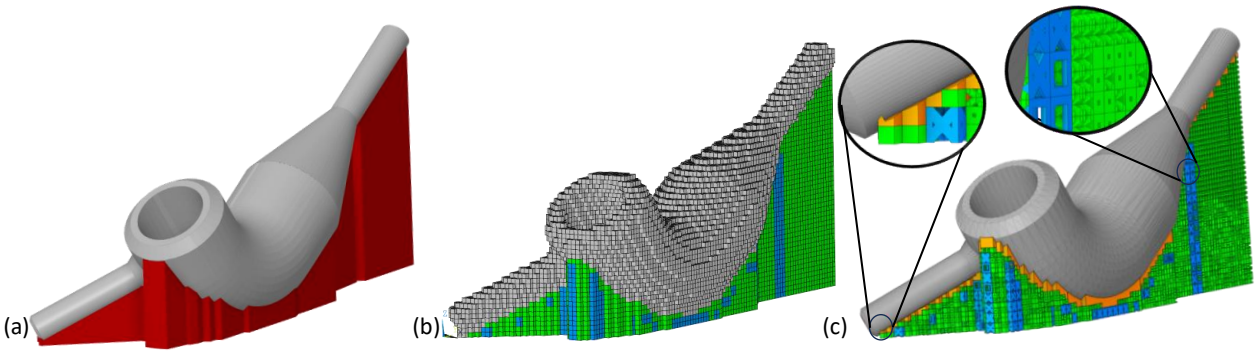

Figure 21: 3D representation of the supercritical carbon dioxide (sCO_2) heat exchanger adapter for the (a) .stl format with predefined support structure (red); (b) voxel mesh with 1-mm (green) and 2-mm (blue) support domains; (c) example of computationally designed structure, $Op_{ex,3}$.

Orientation of the adapter is critical in the fabrication of this part as it cannot have any support structure in the internal channels. In addition to the difficulty of removing such features, internal supports would interfere with the flow of the CO_2. Therefore, the orientation must be pre-set to avoid internal support structure. This results in bounding box dimensions of 105 × 39 × 51 mm (length × width × height). The support structure domain is predefined for solid support using Materialise Magics® to reduce volume. With the design domain established, the objective is to find the optimal distribution of a = 3 2-mm unit cell types (2×2×2 mm^3) and b = 3 1-mm unit cell types (1×1×1 mm^3), shown in Figure 20, for n = 3,194 locations for the unit cells to minimize the heat transfer rate, Q_{in}, into the structure. The maximum stress is defined as the maximum ratio of the p-Norm stress to the yield stress of the material, Eq. (32). Adhering to the 1.5 safety factor for aerospace components [92], the maximum stress is set to 0.66 with p = 8 [80]. With the layer height of 40 μm, U_{max} = 40 μm for the displacement constraints, Eq. (33). The volume constraint is set to V_{max} = 3,808 mm^3, which is a 50% reduction in volume from a completely solid domain.

To begin the pre-optimization stage, the STL of the adapter is inputted into the voxelizer with the voxel size set to 1 mm^3. Next, the 1-mm and 2-mm unit cell locations are identified, as shown in Figure 21(b), resulting in m = 631 2-mm locations and k = 2,563 1-mm locations. With the voxel mesh of all subdomains created, the two part-scale models are run to obtain the ESL for the steady-state thermal and static structural sub-models. An element size and superlayer of 1 mm superlayer thickness is set, yielding 25 combined layers. Volumetric heating, 9.35E13 W/m^3, is applied for 0.4 milliseconds and a cooling of 5 seconds. To represent the dissipation of heat due to convection and radiation, a convection coefficient of 800 $[W/m^2 \cdot ℃]$ is applied to all exposed faces, excluding the base plate. A convection coefficient of 1000 $[W/m^2 \cdot ℃]$ and constant temperature of 200℃ is applied to the base plate. The aggregated temperature distribution at the nodes connecting the transition subdomain to the bulk support subdomain is extracted from the transient thermal analysis. The default support structure utilized for the ISM layer activation is composed of SC 2-mm unit cells and sol 1-mm unit cells to obtain homogenous results. The inherent strain vectors used for this model are ε_{xx} = -0.15, ε_{yy} = -0.15, and ε_{zz} = 0.2 [104], equivalent to those of an Inconel

718, a commonly employed nickel-based superalloy. After all layers have been activated, the forces are extracted as ESL for the static structure analysis for the optimizer, as described in Section 4.4.2.

The hyperparameters for the optimizer are set to $T_0 = 50$ and $\alpha = 0.5$. The initial state is set at the lowest volume, with 2 mm unit cells of SC and 1 mm unit cells of bc. Given the strict volume constraint, beginning at a low volume would allow for more exploration in the earlier stages. To begin the exploration stage, the stage-dependent annealing swapping performs 799 swaps per iteration, equating to the number of design variables, *n/4*. At $T_0/2$, the intermediate stage is reached and the number of swaps changes to *n/40*. Next, the fine-tuning stage is reached at $T_k < 1$, for which the number of swaps changes to *n*/400. There are many types of stopping criteria (e.g., minimum algorithm temperature [66], the objective function tolerance is reached [67], or a set number of iterations [68,69]). The stopping criteria chosen for this demonstration is the maximum number of 850 iterations, associated with 12 hours of run time. To ensure an acceptable solution could be found within this timeframe, the objective function tolerance was also checked to be less than 1% difference. Finally, when the stopping criteria is obtained, the results are compiled and compared to the benchmark designs of uniformly distributed 2 mm unit cells with 1 mm sol.

To capture the average behavior of the heuristic optimizer, the optimization process is run 30 times to obtain a statistical average and standard deviations for the traditional SA, using 8 swaps per iteration, and the method proposed in Section 3.4.5, incorporating the stage-dependent annealing swapping strategy. The iteration histories (i.e., number of function calls) for both optimizers are plotted in Figure 22, showing the change in heat transfer rate through only the support structure. For the traditional SA optimizer, the approximately linear decline of the objective function results in lower heat dissipation than that of the M-SA after the same number of iterations (i.e., function calls). The M-SA shows an exponentially declining trend from the initially proposed state to a linearly declining trend for the average rate of heat transfer, which rapidly reduces the objective function during the exploration stage. Notably, there are $3^{3,194}$ possible configurations, and only 850 are sampled each run, which is an extremely small fraction of the entire design space. However, this optimally directed demonstration shows that the M-SA can consistently converge the

results of 30 runs, with less than 1% difference between the objective functions of the last two iterations. The sensitivity of the method to the randomized swapping and acceptance between the 30 runs is computed by considering the reliability through the computation of the coefficient of variation [93]. For this demonstration, the coefficient of variation is ~1.02%, which indicates good consistency between runs.

To evaluate the quality of the computationally designed structures, the average results are compared to benchmark designs of uniformly distributed 2 mm unit cells (i.e., SC, TR, or FC) with completely solid 1 mm unit cells (i.e., sol). Given the constraints, the average computationally designed structure, $Op_{avg,4}$, and SC Only are the only configurations able to satisfy all the constraints. Despite the 2% difference in volume, the $Op_{avg,4}$ achieves a heat dissipation 16% higher than SC Only and 19% lower maximum deformation in z. Notably, no solid part structure was utilized in the computation of the heat transfer; therefore, all heat flows through the support structure. When printing the physical model, heat would be able to flow through the solid structure connected to the build plate, thereby changing the temperature distribution. By not considering the solid part structure, a built-in safety factor is assumed. Compared to the original completely solid domain which is about 32% of the total cost, the averaged computationally designed results in a reduced cost of 19% of the final build cost. These results indicate that the optimizer can consistently design more cost-efficient configuration solutions by employing multi-sized unit cells.

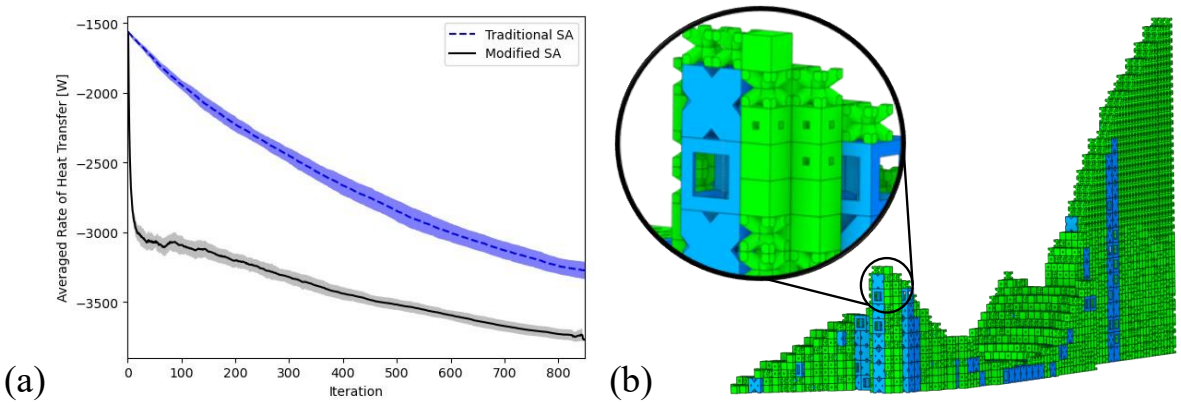

Figure 22: Average objective function values for the heat transfer rate of the traditional SA optimizer and the M-SA for the sCO_2 HX. Shaded regions show standard deviation with (b) an example Op_{ex3}, with final values: Objective = -3,742 W, Volume = 3,807 mm^3, p-Norm = 0.08, U_z = 18.24 mm

Table 10: Comparison of the benchmark results to the average of 30 computationally designed structures for the sCO_2 HX adapter case study, $Op_{avg,3}$, with standard deviations shown in parentheses for the optimizer.

	$\|Q_{in}\|$	V(x)	P-norm Stress	Max(U_z) [μm]	SC/TR/FC sc/bv/sol	V(x) < 3,808 P-norm < 0.66 Max(U_z)< 40
Solid	6470	7617	0.053	4.6	--	No
SC Only	3182	3711	0.166	19.45	631/0/0 0/0/2,563	Yes
TR Only	3756	4468	0.108	13.07	0/631/0 0/0/2,563	No
FC Only	4775	4891	0.072	8.08	0/0/1,776 0/0/2,563	No
$Op_{avg,3}$	3,742 (38)	3,802 (8.8)	0.087 (0.004)	16.0 (0.51)	151/185/295 645/1,228/689 (6/12/11/18/16/21)	Yes

Validation of the ESL performed for an example for $Op_{ex,3,}$ which has an objective function equivalent to the average ($Op_{avg,3}$), by comparing the part scale model results to benchmark structures. The input for the ESL for the structural loading is the average nodal force load from the part applied at the interface of the support structure. The structure utilized to obtain those results is composed of the weakest of the unit cell sizes, SC-bc (i.e., 2 mm SC and 1 mm bc). It is expected that a hybrid lattice support structure would have a lower deformation. After executing the part-scale ISM for both the SC-bc and the $Op_{ex,3}$, the results show only a 3% reduction in max deformation compared to SC-bc. Compared to the deformation results shown with the aerospace bracket in Chapter 3, the percentage difference is smaller. This may be attributed to the number of iterations that were run and the constraints chosen. The trend of the iteration history shows that the optimizer has not reached a steady-state value, therefore, more iterations may be needed to find an optimal solution. The constraints also limit the design space for this structure given the strict, 50% volume constraint. Therefore, running more iterations will not guarantee finding the global optimum or a high percentage difference in the computationally designed lattice support structure, compared to the benchmark designs. In summary, this demonstration does show that the method creates the opportunity for lattice

support structure design for complex geometries. Further work will be needed to affirm the proposed method using physical models.

4.6. Conclusions

By optimizing the configuration of a hybrid lattice support structure with multi-sized unit cells, manufacturing cost reductions are achieved. In this work, a multi-sized unit cell approach is presented using voxel-mesh representation to connect lattice support structures to complex structures. Once identified, M-SA is employed to search for an optimal solution. The combination of the approximation techniques (i.e., ESL and HA) and stage-dependent annealing swapping strategy of M-SA, allow for the efficient search of the design domain within 800 iterations. The approach is demonstrated for the case study of a sCO_2 heat exchange adapter, made of nickel-based superalloy: Hanyes 282. With the volume and structural constraints satisfied, the average computationally designed structure and the SC Only, composed of 2 mm SC and 1 mm solid unit cells, are compared. The hybrid lattice support structure generated by the method generates 16% better heat dissipation. When validating the approximation methods of ESL and HA, the static structural results indicate that the method shows promise in creating better structures, but more iterations will be needed for conclusive results.

5. Conclusions, Contributions, and Areas for Future Work

5.1. Overview

Laser Powder Bed Fusion (LPBF) is a popular metal additive manufacturing technique that manufactures components by fusing microscopic layers of powders with a high-power energy source. Due to the rapid thermal cycle and low thermal conductivity of the powder, support structures are necessary for overhang features. Lattices are a promising solution as they are composed of self-supporting unit cells with tailorable properties. Despite the promise of lattices as viable support structures in LPBF, there are still obstacles hindering their widespread use. In this work, two questions were posed and addressed regarding (1) the high computational cost of finding optimally directed solutions, and (2) the inability to apply lattice support structures to complex geometries. To this end, a modified-simulated annealing-based method (M-SA) and multi-sized unit cell approach are proposed.

The first question asks: how can designers *efficiently* find an optimally directed lattice support structure solution that improves heat dissipation while satisfying multiple AM constraints for LPBF? Hence, a modified simulated annealing-based method is introduced to efficiently design lattice support structures for maximum heat dissipation while considering AM design constraints (e.g., structural integrity, material cost, and post-processing). Reduced iteration count required for design exploration is achieved with the introduction of the stage-dependent annealing swapping strategy. Furthermore, costly simulation-informed evaluations are mitigated with the addition of a pre-defined library of unit cells, equivalent static loading (ESL), and homogenization approximation (HA). Preliminary results used to investigate the design of thermally conductive lattice support structures constrained by material and post-processing costs for a cantilever beam were first executed in Chapter 2. The method was shown to achieve an average of 16% better heat dissipation than the uniformly distributed benchmark designs, with manufacturing constraints satisfied. Next, the addition of structural limitations on deformation and residual stress were applied. Two case studies, a cantilever beam and an aerospace bracket, validated the method by demonstrating material

cost savings of up to 61% and post-processing cost savings of up to 62% when compared to a solid support domain, with manufacturing constraints satisfied. These results show the feasibility of the method to generate lattice support structures at reduced computational cost for horizontal surfaces.

Connecting lattice support structures to curved or inclined surfaces has also been shown to be a major roadblock in their widespread adoption due to high computational costs. Therefore, the second question asks, how can lattice support structures be computationally designed to be *attached* to complex structures? To this end, a multi-sized unit cell approach is presented to automate the locations of multi-sized unit cells. By utilizing voxel modeling, the size of the bulk support subdomain can be increased with multi-sized unit cells. When coupled with M-SA, the approach can be employed to efficiently design lattice support structures for complex geometries. This is validated with the case study of a supercritical carbon dioxide heat exchanger adapter pipe. Results show a 16% increase in heat dissipation and a 19% decrease in distortion when compared to the single-sized unit cell benchmark design that also satisfied the constraints.

5.2. Contributions

This dissertation contributes to the broader field of engineering design and methodology for additive manufacturing in these areas:

1. Introducing a method to increase the efficiency of stochastic optimizers by reducing computational costs.
2. Establishing a method to incorporate both thermal and structural simulation-informed evaluations for lattice support structures.
3. Developing an approach to broaden the application of lattice support structure to complex geometries.

5.3. Areas for Future Work

While this work addresses several limitations with existing global optimizers, the interdisciplinary features (e.g., finite element modeling, homogenization approximation, discrete optimization) create opportunities for future research. In this subsection, potential directions are presented.

5.3.1. Evaluating other priority factors

Optimizers allow designers to make informed decisions on how to maximize priority factors in manufacturing designs such as efficiency and profit. The M-SA proposed aims to create the foundation for more sophisticated optimization approaches to aid in the design for additive manufacturing. Four inequality constraints are provided in this work, but users can include other constraint(s) based on their practical needs.

Several assumptions were made regarding the computational fabrication of the entire build which can be further investigated to match the physical fabrication. A major simplification was that an ideal lattice structure was manufactured, and it is reacting to a non-ideal part. However, research has shown that unit cells possess many defects that would change their material and geometric properties [40,105]. Incorporating those defects would enable better predictions of the macroscopic lattice structure. For example, the horizontal struts accumulate material as it is a small overhang feature. This would change the amount of volume a unit cell, like the simple cubic unit cell, would have. By considering the geometric accuracy of the unit cell, the volume can be better approximated. This will also be important when considering printability as the transition between geometrically different unit cells is critical for reducing intracellular stress [55] and can increase the uniform distribution of temperature.

Other constraints that consider the printability would be regarding time. Build time is associated with manufacturing costs as it increases overhead costs [14,103]. For instance, a trade-off of using smaller unit cells for increased physical properties is the increase in build time [21,62,106]. This is attributed to the movement of the laser to create the cross-sectional area. Another aspect of time that can be included is the time to dissipate heat [18]. Although the equivalent static loading was utilized to approximate the evolving heat dissipation of the transient thermal part scale model [51], ensuring that the support structure dissipates heat within a constrained period would also reduce the build time such that each layer can be applied within an appropriate time frame. The configuration of struts in a unit cell will have a direct impact on the amount of time to dissipate heat [60]. Furthermore, the investigation into the fraction of heat flow through the solid

parts versus the support structure domain would also be of interest for uniform heat distribution. If more heat is directed to the solid part, accumulation of heat may occur and lead to part damage.

In Chapter 3, the deformation in the x- and y-axes (U_x and U_y) was considered given the functionality of the aerospace bracket to brace additional components. By including these constraints, a better solution is found. Future work can explore additional functionalities of the part as design constraints. For example, the adapter used in the Chapter 4 case study could include a constraint on pressure drop and heat exchange performance to ensure quality parts are created [85,86]. Notably, the inclusion of other simulation-informed evaluations would require increased computational costs, especially when considering the part that is not currently modeled in the design. Therefore, modifications to M-SA would be needed, such as weakly coupling the results of the support structure to the analysis of the part.

5.3.2. Guidelines for user-defined constraints

The method presented in this work aims to help with the widespread application of lattice support structures. However, many user-defined parameters were introduced but not fully investigated. Future work regarding these parameters are areas of interest.

To reduce computational costs between iterations, a pre-defined library of unit cells is employed. These cells, 0.1 to 10 mm [40,53], can be divided into two categories: strut and surface-based [40]. Strut-based unit cells, such as the body-centered cell [4,40,55], can be defined using configurations of beams and nodes. Surface-based unit cells, such as gyroids [15,107], are defined mathematically using isosurfaces connected at points. Although both have been utilized for design optimization of lattices, strut-based unit cells are the most popular [4,40]. Knowledge regarding how to choose the appropriate unit cells would help designers with varying levels of experience. Previous works have divided basic unit cell geometries into families [53,57] or used topology optimization to create unit cells [21,53,100]. Both methods result in many variations of unit cells that possess properties (e.g., geometric, material, and structural) that could be advantageous, depending on the need. Based on the current method, these advanced libraries can be incorporated into the design. However, a library full of hundreds of designs [57] would increase the number

of possible configurations exponentially [53], resulting in a redefinition of the stages. Therefore, guidelines would be needed to simplify the unit cell selection based on need, printability [55,57], connectivity [57–59], and the chosen optimizer [53].

The method solves the static thermal and structural analyses at each iteration, therefore the equivalent static loads are imperative to find a solution. Future research could explore the appropriate part-scale models and equivalent static loads. One example would be the inherent strain method (ISM), which requires structure underneath the overhang to provide accurate results. Currently, the nodal forces are extracted from the part using the weakest unit cell combination. However, this makes the reaction forces independent of the actual design. It may be more useful to run the part-scale every few iterations to ensure the loading is representative of the configuration.

The stage-dependent annealing swapping strategy is one of the major contributions of this work. It was shown to increase design exploration at lower iteration counts. This strategy requires designers to understand how to identify the three stages and how many swaps to apply. The current approach to identifying the stages is based on the frequency of the probability of acceptance for a constant swapping approach. This requires an additional step within the process that is highly dependent on the hyperparameters. A more systematic approach is needed to provide guidelines for users to define the stages based on selected hyperparameters. More questions also arise regarding the number of stages needed and corresponding swaps. For example, this work changes the number of swaps in a pre-set declining manner but having an adaptive change in the number of swaps may be necessary, similar to the adaptive annealing schedule [66]. Furthermore, future work could investigate the impact factor of the number of swaps on the model's ability to reach an optimal state.

5.3.3. Additional Validation

Computationally designed configurations of lattice support structures were generated for three case studies of varying complexity: cantilever beam, aerospace bracket, and heat exchanger adapter pipe. The method was computationally validated against the traditional simulated annealer (SA) and benchmark

designs. However, other forms of validation are needed before broadened application. The two basic forms of validation come both computationally and physically.

Although this work focuses on the modifications made to SA, other gradient and non-gradient-based optimizers can be employed for comparison and may benefit from some aspects of the proposed method. Comparison with gradient-based optimizers could be performed in one of two ways: comparing to other lattice support structure methods or the comparison to the standard material distribution of an arbitrary domain space. For a more accurate comparison, the objective function should be the same for all the models. However, the approach must also be competitive with the popular material distribution methods [13] which require a differentiable objective function. Therefore, additional objective functions will be needed, such as the minimization of thermal potential energy [37,38], thermal compliance [13,39], average temperature [30], and thermal gradient. Furthermore, gradient-based optimizers, such as the method of moving asymptotes [18], perform a localized search of the design domain to find a solution. By incorporating the proposed stage-dependent annealing swapping, an increased search of the design domain may occur. Alternatively, non-gradient-based optimizers, such as genetic algorithms (GAs) [20,108] and particle swarm method (PSO) [109] are known for increased design exploration [42]. A direct comparison of the computational cost (e.g., number of iterations) can be performed to determine which problems are better suited for lattice support structure design.

The outcome of the physical model is highly dependent on the material and printing parameters which are difficult to incorporate into the simulation. Two materials were explored in this work: AlSi10Mg and Haynes 282. The commonly printed aluminum alloy has a high thermal conductivity, allowing for high dissipation of heat. Whereas, nickel-based superalloys are known to undergo cracking due to their low thermal conductivity and high thermal expansion coefficient [40]. Although the material properties are included within the inherent strain method (ISM); the inherent strain vectors are dependent on the material compositions and printing parameters [82,87,110]. Therefore, calibration of the model should be included within the workflow of the proposed M-SA. Calibration can be performed empirically by printing coupons

[111–113], such as cantilever beams, that are cut and measured for deformity. Regression models can then be employed to find the inherent strain vectors that would match the physical deformation of the coupons to the simulated deformations. Calibrated inherent strain vectors for the bulk and all pre-defined unit cells provide a better approximation of the printed structural properties [17]. Furthermore, stress relief annealing constraints could be considered based on the calibrated ISM results [114], which is an important aspect of post-processing within AM of metal components [1].

5.4. Coda

This dissertation proposes and validates a modified-simulation annealing-based method (M-SA) to efficiently design multi-functional lattice support structures. By introducing a stage-dependent annealing swapping strategy, design exploration is expedited through reduced iteration count. Homogenization approximation and equivalent static loading are also shown to reduce computational cost between each iteration at multiple scales and complexities. Coupled with a multi-sized unit cell approach, M-SA is also applicable to complex geometries (i.e., structures with curved surfaces and inclines). The proposed method seeks to equip designers with an alternative approach to designing quality lattice support structures at lower computational costs. This is particularly beneficial within the additive manufacturing market as it needs to be competitive against other well-established manufacturing markets for continued usage [1,94]. Thus, this work shows promise in reducing manufacturing costs and computational costs. Notably, this work is not complete as additional research is required before widespread application. Future work investigating the method's inputs (e.g., constraint choice) and outputs (e.g., physical validation) would enhance the findings of this dissertation.

6. References

[1] Vafadar, A., Guzzomi, F., Rassau, A., and Hayward, K., 2021, "Advances in Metal Additive Manufacturing: A Review of Common Processes, Industrial Applications, and Current Challenges," Applied Sciences, 11(3), p. 1213.

[2] Grasso, M., and Colosimo, B. M., 2017, "Process Defects and in Situ Monitoring Methods in Metal Powder Bed Fusion: A Review," Measurement Science and Technology, 28(4), p. 044005.

[3] Paul, R., and Anand, S., 2015, "Optimization of Layered Manufacturing Process for Reducing Form Errors with Minimal Support Structures," Journal of Manufacturing Systems, 36, pp. 231–243.

[4] Nazir, A., Abate, K. M., Kumar, A., and Jeng, J.-Y., 2019, "A State-of-the-Art Review on Types, Design, Optimization, and Additive Manufacturing of Cellular Structures," International Journal of Advanced Manufacturing Technology, 104(9), pp. 3489–3510.

[5] Park, S., and Rosen, D. W., 2016, "Quantifying Effects of Material Extrusion Additive Manufacturing Process on Mechanical Properties of Lattice Structures Using As-Fabricated Voxel Modeling," Additive Manufacturing, 12, pp. 265–273.

[6] Zhang, B., Li, Y., and Bai, Q., 2017, "Defect Formation Mechanisms in Selective Laser Melting: A Review," Chinese Journal of Mechanical Engineering, 30(3), pp. 515–527.

[7] Javidrad, H. R., and Javidrad, F., 2023, "Review of State-of-the-Art Research on the Design and Manufacturing of Support Structures for Powder-Bed Fusion Additive Manufacturing," Prog Addit Manuf.

[8] Jiang, J., Xu, X., and Stringer, J., 2018, "Support Structures for Additive Manufacturing: A Review," Journal of Manufacturing and Materials Processing, 2(4), p. 64.

[9] Thomas, D., and Gilbert, S., 2014, *Costs and Cost Effectiveness of Additive Manufacturing: A Literature Review and Discussion*, 1176, NIST special publication.

[10] Hao, L., Raymont, D., Chunze, Y., Hussein, A., and Young, P., eds., 2011, "Design and Additive Manufacturing of Cellular Lattice Structures," *Innovative Developments in Virtual and Physical Prototyping*, CRC Press, Leiria, Portugal, pp. 249–254.

[11] Mirzendehdel, A. M., and Suresh, K., 2016, "Support Structure Constrained Topology Optimization for Additive Manufacturing," Computer-Aided Design, 81, pp. 1–13.

[12] Craeghs, T., Clijsters, S., Kruth, Jean.-P., Bechmann, F., and Ebert, Marie.-C., 2012, "Detection of Process Failures in Layerwise Laser Melting with Optical Process Monitoring," Physics Procedia, 39, pp. 753–759.

[13] Huang, R., Dai, N., Cheng, X., and Wang, L., 2020, "Topology Optimization of Lattice Support Structures for Heat Conduction in Selective Laser Melting," International Journal of Advanced Manufacturing Technology, 109(7–8), pp. 1841–1851.

[14] Ravichander, B. B., Thakare, S., Ganesh-Ram, A., Farhang, B., Hanumantha, M., Yang, Y., Shayesteh Moghaddam, N., and Amerinatanzi, A., 2021, "Cost-Aware Design and Fabrication of New Support Structures in Laser Powder Bed Fusion: Microstructure and Metallurgical Properties," Applied Sciences, 11(21), p. 10127.

[15] Hussein, A., Hao, L., Yan, C., Everson, R., and Young, P., 2013, "Advanced Lattice Support Structures for Metal Additive Manufacturing," Journal of Materials Processing Technology, 213(7), pp. 1019–1026.

[16] Cheng, L., Liang, X., Bai, J., Chen, Q., Lemon, J., and To, A., 2019, "On Utilizing Topology Optimization to Design Support Structure to Prevent Residual Stress Induced Build Failure in Laser Powder Bed Metal Additive Manufacturing," Additive Manufacturing, 27, pp. 290–304.

[17] Tran, H. T., Liang, X., and To, A. C., 2020, "Efficient Prediction of Cracking at Solid-Lattice Support Interface during Laser Powder Bed Fusion via Global-Local J-Integral Analysis Based on Modified Inherent Strain Method and Lattice Support Homogenization," Additive Manufacturing, 36, p. 101590.

[18] Lee, K.-Hyun., and Yun, G. J., 2022, "Design Optimization of Thermally Conductive Support Structure for Laser Powder-Bed Fusion Process with Part-Scale Thermal History," Additive Manufacturing, 51, p. 102627.
[19] Vaissier, B., Pernot, J.-P., Chougrani, L., and Véron, P., 2019, "Genetic-Algorithm Based Framework for Lattice Support Structure Optimization in Additive Manufacturing," Computer-Aided Design, 110, pp. 11–23.
[20] Feng, R., Liu, F., Xu, W., Ma, M., and Liu, Y., 2016, "Topology Optimization Method of Lattice Structures Based on a Genetic Algorithm," International Journal of Steel Structures, 16(3), pp. 743–753.
[21] Boos, E., Ihlenfeldt, S., Milaev, N., Bruns, M., and Elsner, B. A. M., 2023, "Simulation-Based Support Generation for Laser Powder Bed Fusion Processes," 3D Printing and Additive Manufacturing, 10(2), pp. 173–182.
[22] Tran, H. T., and To, A. C., 2023, "Cracking Prediction at Solid-Tooth Support Interface during Laser Powder Bed Fusion Additive Manufacturing," Journal of Science: Advanced Materials and Devices, 8(4), p. 100615.
[23] Tran, H. T., Chen, Q., Mohan, J., and To, A. C., 2020, "A New Method for Predicting Cracking at the Interface between Solid and Lattice Support during Laser Powder Bed Fusion Additive Manufacturing," Additive Manufacturing, 32, p. 101050.
[24] Bobbio, L. D., Qin, S., Dunbar, A., Michaleris, P., and Beese, A. M., 2017, "Characterization of the Strength of Support Structures Used in Powder Bed Fusion Additive Manufacturing of Ti-6Al-4V," Additive Manufacturing, 14, pp. 60–68.
[25] Krol, T. A., Zaeh, M. F., and Seidel, C., "Optimization of Supports in Metal-Based Additive Manufacturing by Means of Finite Element Models."
[26] Bartsch, K., Ohrenberg, J., and Emmelmann, C., 2020, "Benchmark Parts for the Evaluation of Optimized Support Structures in Laser Powder Bed Fusion of Metals," Procedia CIRP, 94, pp. 254–259.
[27] Leary, M., Maconachie, T., Sarker, A., Faruque, O., and Brandt, M., 2019, "Mechanical and Thermal Characterisation of AlSi10Mg SLM Block Support Structures," Materials & Design, 183, p. 108138.
[28] Malekipour, E., Tovar, A., and El-Mounayri, H., 2018, "Heat Conduction and Geometry Topology Optimization of Support Structure in Laser-Based Additive Manufacturing," *Mechanics of Additive and Advanced Manufacturing, Volume 9*, J. Wang, B. Antoun, E. Brown, W. Chen, I. Chasiotis, E. Huskins-Retzlaff, S. Kramer, and P.R. Thakre, eds., Springer International Publishing, Cham, pp. 17–27.
[29] White, L., Liang, X., Zhang, G., Cagan, J., and Zhang, Y. J., 2023, "Coupling Simulated Annealing and Homogenization to Design Thermally Conductive Hybrid Lattice Support Structures for LPBF," ASME International Design Engineering Technical Conference & Computers and Information in Engineering Conference (IDETC/CIE). Boston, MA. Aug 20-23, 2023.
[30] Bartsch, K., Herzog, D., Emmelmann, C., and Lange, F., 2019, "A Novel Approach to Support Structures Optimized for Heat Dissipation in SLM by Combining Process Simulation with Topology Optimization," The NAFEMS World Congress Quebec City, Quebec, QC, Canada.
[31] Li, C., Liu, J. F., Fang, X. Y., and Guo, Y. B., 2017, "Efficient Predictive Model of Part Distortion and Residual Stress in Selective Laser Melting," Additive Manufacturing, 17, pp. 157–168.
[32] Liang, X., White, L., Cagan, J., Rollett, A. D., and Zhang, Y. J., 2023, "Unit-Based Design of Cross-Flow Heat Exchangers for LPBF Additive Manufacturing," Journal of Mechanical Design, 145(1), p. 012002.
[33] Ameen, W., Mohammed, M. K., Al-Ahmari, A., Ahmed, N., and Mian, S. H., 2020, "Investigation of Support Structure Parameters and Their Affects during Additive Manufacturing of Ti6Al4V Alloy via Electron Beam Melting," Proceedings of the Institution of Mechanical Engineers, Part L: Journal of Materials: Design and Applications, p. 1464420720981668.

[34] Chen, H., Gu, D., Xiong, J., and Xia, M., 2017, "Improving Additive Manufacturing Processability of Hard-to-Process Overhanging Structure by Selective Laser Melting," Journal of Materials Processing Technology, 250, pp. 99–108.
[35] Triantaphyllou, A., Giusca, C. L., Macaulay, G. D., Roerig, F., Hoebel, M., Leach, R. K., Tomita, B., and Milne, K. A., 2015, "Surface Texture Measurement for Additive Manufacturing," Surf. Topogr.: Metrol. Prop., 3(2), p. 024002.
[36] Dbouk, T., 2017, "A Review about the Engineering Design of Optimal Heat Transfer Systems Using Topology Optimization," Applied Thermal Engineering, 112, pp. 841–854.
[37] Cheng, L., Liu, J., Liang, X., and To, A. C., 2018, "Coupling Lattice Structure Topology Optimization with Design-Dependent Feature Evolution for Additive Manufactured Heat Conduction Design," Computer Methods in Applied Mechanics and Engineering, 332, pp. 408–439.
[38] Cheng, L., Liu, J., and To, A. C., 2018, "Concurrent Lattice Infill with Feature Evolution Optimization for Additive Manufactured Heat Conduction Design," Structural and Multidisciplinary Optimization, 58(2), pp. 511–535.
[39] Lohan, D. J., Dede, E. M., and Allison, J. T., 2020, "A Study on Practical Objectives and Constraints for Heat Conduction Topology Optimization," Structural and Multidisciplinary Optimization, 61(2), pp. 475–489.
[40] Echeta, I., Feng, X., Dutton, B., Leach, R., and Piano, S., 2020, "Review of Defects in Lattice Structures Manufactured by Powder Bed Fusion," International Journal of Advanced Manufacturing Technology, 106(5–6), pp. 2649–2668.
[41] Porter, J. M., Larsen, M. E., and Howell, J. R., 2009, "Discrete Optimization of Radiant Heaters with Simulated Annealing," American Society of Mechanical Engineers Digital Collection, pp. 903–908.
[42] Eberhard, P., Schiehlen, W., and Bestle, D., 1999, "Some Advantages of Stochastic Methods in Multicriteria Optimization of Multibody Systems," Archive of Applied Mechanics, 69(8), pp. 543–554.
[43] Dos Reis, F., and Karathanasopoulos, N., 2022, "Inverse Metamaterial Design Combining Genetic Algorithms with Asymptotic Homogenization Schemes," International Journal of Solids and Structures, 250, p. 111702.
[44] Liang, X., To, A. C., Du, J., and Zhang, Y. J., 2021, "Topology Optimization of Phononic-like Structures Using Experimental Material Interpolation Model for Additive Manufactured Lattice Infills," Computer Methods in Applied Mechanics and Engineering, 377, p. 113717.
[45] Vaidya, R., and Anand, S., 2016, "Optimum Support Structure Generation for Additive Manufacturing Using Unit Cell Structures and Support Removal Constraint," Procedia Manufacturing, 5, pp. 1043–1059.
[46] Kuo, Y.-H., Cheng, C.-C., Lin, Y.-S., and San, C.-H., 2018, "Support Structure Design in Additive Manufacturing Based on Topology Optimization," Structural and Multidisciplinary Optimization, 57(1), pp. 183–195.
[47] Pandey, H. M., Chaudhary, A., and Mehrotra, D., 2014, "A Comparative Review of Approaches to Prevent Premature Convergence in GA," Applied Soft Computing, 24, pp. 1047–1077.
[48] Kirkpatrick, S., Gelatt, C. D., and Vecchi, M. P., 1983, "Optimization by Simulated Annealing," Science, 220(4598), pp. 671–680.
[49] Lee, G., Joo, Y., and Kim, S. J., 2021, "On the Objective Function for Topology Optimization of Heat Sinks," IEEE Transactions on Components, Packaging and Manufacturing Technology, 11(11), pp. 1776–1782.
[50] Cao, Q., Bai, Y., Zheng, Z., Zhang, J., Fuh, J. Y. H., and Wang, H., 2022, "Support Removal on Thin-Walled Parts Produced by Laser Powder Bed Fusion," 3D Printing and Additive Manufacturing.
[51] Subedi, S. C., Shahba, A., Thevamaran, M., Thoma, D. J., and Suresh, K., 2022, "Towards the Optimal Design of Support Structures for Laser Powder Bed Fusion-Based Metal Additive Manufacturing via Thermal Equivalent Static Loads," Additive Manufacturing, 57, p. 102956.

[52] Subasi, A., Sahin, B., and Kaymaz, I., 2016, "Multi-Objective Optimization of a Honeycomb Heat Sink Using Response Surface Method," International Journal of Heat and Mass Transfer, 101, pp. 295–302.
[53] Nguyen, J., Park, S.-I., Rosen, D. W., Folgar, L., and Williams, J., 2012, "Conformal Lattice Structure Design and Fabrication." 2012 International Solid Freeform Fabrication Symposium. University of Texas at Austin, 2012.
[54] Deshpande, V. S., Fleck, N. A., and Ashby, M. F., 2001, "Effective Properties of the Octet-Truss Lattice Material," Journal of the Mechanics and Physics of Solids, 49(8), pp. 1747–1769.
[55] Kang, D., Park, S., Son, Y., Yeon, S., Kim, S. H., and Kim, I., 2019, "Multi-Lattice Inner Structures for High-Strength and Light-Weight in Metal Selective Laser Melting Process," Materials & Design, 175, p. 107786.
[56] Melancon, D., Bagheri, Z. S., Johnston, R. B., Liu, L., Tanzer, M., and Pasini, D., 2017, "Mechanical Characterization of Structurally Porous Biomaterials Built via Additive Manufacturing: Experiments, Predictive Models, and Design Maps for Load-Bearing Bone Replacement Implants," Acta Biomaterialia, 63, pp. 350–368.
[57] Liu, Y., Zhuo, S., Xiao, Y., Zheng, G., Dong, G., and Zhao, Y. F., 2020, "Rapid Modeling and Design Optimization of Multi-Topology Lattice Structure Based on Unit-Cell Library," Journal of Mechanical Design, 142(091705).
[58] Sanders, E. D., Pereira, A., and Paulino, G. H., 2021, "Optimal and Continuous Multilattice Embedding," Science Advances, 7(16), p. eabf4838.
[59] Baldwin, M., Meisel, N. A., and McComb, C., 2022, "A Data-Driven Approach for Multi-Lattice Transitions." 2022 International Solid Freeform Fabrication Symposium. University of Texas at Austin, 2022.
[60] Downing, D., Leary, M., McMillan, M., Alghamdi, A., and Brandt, M., 2020, "Heat Transfer in Lattice Structures during Metal Additive Manufacturing: Numerical Exploration of Temperature Field Evolution," Rapid Prototyping Journal, 26(5), pp. 911–928.
[61] Miki, T., and Nishiwaki, S., 2022, "Topology Optimization of the Support Structure for Heat Dissipation in Additive Manufacturing," Finite Elements in Analysis and Design, 203, p. 103708.
[62] Hassani, B., and Hinton, E., 1998, "A Review of Homogenization and Topology Optimization I—Homogenization Theory for Media with Periodic Structure," Computers & Structures, 69(6), pp. 707–717.
[63] Zeng, K., Pal, D., Teng, C., and Stucker, B. E., 2015, "Evaluations of Effective Thermal Conductivity of Support Structures in Selective Laser Melting," Additive Manufacturing, 6, pp. 67–73.
[64] Nguyen, J., Park, S., and Rosen, D., 2013, "Heuristic Optimization Method for Cellular Structure Design of Light Weight Components," International Journal of Precision Engineering and Manufacturing, 14(6), pp. 1071–1078.
[65] Salonitis, K., Chantzis, D., and Kappatos, V., 2017, "A Hybrid Finite Element Analysis and Evolutionary Computation Method for the Design of Lightweight Lattice Components with Optimized Strut Diameter," International Journal of Advanced Manufacturing Technology, 90(9), pp. 2689–2701.
[66] Triki, E., Collette, Y., and Siarry, P., 2005, "A Theoretical Study on the Behavior of Simulated Annealing Leading to a New Cooling Schedule," European Journal of Operational Research, 166(1), pp. 77–92.
[67] Yadav, R., Tripathi, S., Asati, S., and Das, M. K., 2020, "A Combined Neural Network and Simulated Annealing Based Inverse Technique to Optimize the Heat Source Control Parameters in Heat Treatment Furnaces," Inverse Problems in Science and Engineering, 28(9), pp. 1265–1286.
[68] Lundy, M., and Mees, A., 1986, "Convergence of an Annealing Algorithm," Mathematical Programming, 34(1), pp. 111–124.

[69] Puentes, L., Cagan, J., and McComb, C., 2020, "Heuristic-Guided Solution Search Through a Two-Tiered Design Grammar," Journal of Computing and Information Science in Engineering, 20(1), p. 011008.
[70] Wang, D., Wei, X., Liu, J., Xiao, Y., Yang, Y., Liu, L., Tan, C., Yang, X., and Han, C., 2022, "Lightweight Design of an AlSi10Mg Aviation Control Stick Additively Manufactured by Laser Powder Bed Fusion," Rapid Prototyping Journal, 28(10), pp. 1869–1881.
[71] Gouge, M., Denlinger, E., Irwin, J., Li, C., and Michaleris, P., 2019, "Experimental Validation of Thermo-Mechanical Part-Scale Modeling for Laser Powder Bed Fusion Processes," Additive Manufacturing, 29, p. 100771.
[72] Xu, S., Liu, J., and Ma, Y., 2022, "Residual Stress Constrained Self-Support Topology Optimization for Metal Additive Manufacturing," Computer Methods in Applied Mechanics and Engineering, 389, p. 114380.
[73] Xiaohui, J., Chunbo, Y., Honglan, G., Shan, G., and Yong, Z., 2022, "Effect of Supporting Structure Design on Residual Stresses in Selective Laser Melting of AlSi10Mg," International Journal of Advanced Manufacturing Technology, 118(5–6), pp. 1597–1608.
[74] Pellens, J., Lombaert, G., Michiels, M., Craeghs, T., and Schevenels, M., 2020, "Topology Optimization of Support Structure Layout in Metal-Based Additive Manufacturing Accounting for Thermal Deformations," Structural and Multidisciplinary Optimization, 61(6), pp. 2291–2303.
[75] Reddy, J. N., and Gartling, D. K., 2010, *The Finite Element Method in Heat Transfer and Fluid Dynamics*, Taylor & Francis Group, Bosa Roca, United States.
[76] Rothwell, A., 2017, "Optimization With Finite Element Analysis," *Optimization Methods in Structural Design*, A. Rothwell, ed., Springer International Publishing, Cham, pp. 283–296.
[77] Langelaar, M., 2018, "Combined Optimization of Part Topology, Support Structure Layout and Build Orientation for Additive Manufacturing," Structural and Multidisciplinary Optimization, 57(5), pp. 1985–2004.
[78] Zhang, Z.-D., Ibhadode, O., Ali, U., Dibia, C. F., Rahnama, P., Bonakdar, A., and Toyserkani, E., 2020, "Topology Optimization Parallel-Computing Framework Based on the Inherent Strain Method for Support Structure Design in Laser Powder-Bed Fusion Additive Manufacturing," Int J Mech Mater Des, 16(4), pp. 897–923.
[79] Misiun, G., van de Ven, E., Langelaar, M., Geijselaers, H., van Keulen, F., van den Boogaard, T., and Ayas, C., 2021, "Topology Optimization for Additive Manufacturing with Distortion Constraints," Computer Methods in Applied Mechanics and Engineering, 386, p. 114095.
[80] Holmberg, E., Torstenfelt, B., and Klarbring, A., 2013, "Stress Constrained Topology Optimization," Structural and Multidisciplinary Optimization, 48(1), pp. 33–47.
[81] Le, C., Norato, J., Bruns, T., Ha, C., and Tortorelli, D., 2010, "Stress-Based Topology Optimization for Continua," Structural and Multidisciplinary Optimization, 41(4), pp. 605–620.
[82] Liang, X., Cheng, L., Chen, Q., Yang, Q., and To, A. C., 2018, "A Modified Method for Estimating Inherent Strains from Detailed Process Simulation for Fast Residual Distortion Prediction of Single-Walled Structures Fabricated by Directed Energy Deposition," Additive Manufacturing, 23, pp. 471–486.
[83] Sulaiman, S., Hamouda, A. M. S., Abedin, S., and Osman, M. R., 2000, "Simulation of Metal Filling Progress during the Casting Process," Journal of Materials Processing Technology, 100(1), pp. 224–229.
[84] Yuan, M. G., and Ueda, Y., 1996, "Prediction of Residual Stresses in Welded T- and I-Joints Using Inherent Strains," Journal of Engineering Materials and Technology, 118(2), pp. 229–234.
[85] Liang, X., White, L., Cagan, J., Rollett, A. D., and Zhang, Y. J., 2022, "Design and Printability Evaluation of Heat Exchangers for Laser Powder Bed Fusion Process," ASME International Design Engineering Technical Conference & Computers and Information in Engineering Conference (IDETC/CIE). St. Louis, MI. Aug 14-17, 2022.

[86] Liang, X., Li, A., Rollett, A. D., and Zhang, Y. J., 2022, "An Isogeometric Analysis-Based Topology Optimization Framework for 2D Cross-Flow Heat Exchangers with Manufacturability Constraints," Engineering with Computers, 38(6), pp. 4829–4852.
[87] Cheng, L., Bai, J., and To, A. C., 2019, "Functionally Graded Lattice Structure Topology Optimization for the Design of Additive Manufactured Components with Stress Constraints," Computer Methods in Applied Mechanics and Engineering, 344, pp. 334–359.
[88] Liang, X., Dong, W., Hinnebusch, S., Chen, Q., Tran, H. T., Lemon, J., Cheng, L., Zhou, Z., Hayduke, D., and To, A. C., 2020, "Inherent Strain Homogenization for Fast Residual Deformation Simulation of Thin-Walled Lattice Support Structures Built by Laser Powder Bed Fusion Additive Manufacturing," Additive Manufacturing, 32, p. 101091.
[89] Dong, G., Tang, Y., and Zhao, Y. F., 2017, "A Survey of Modeling of Lattice Structures Fabricated by Additive Manufacturing," Journal of Mechanical Design, 139(100906).
[90] Suman, B., and Kumar, P., 2006, "A Survey of Simulated Annealing as a Tool for Single and Multiobjective Optimization," Journal of the Operational Research Society, 57(10), pp. 1143–1160.
[91] Metropolis, N., Rosenbluth, A. W., Rosenbluth, M. N., Teller, A. H., and Teller, E., 1953, "Equation of State Calculations by Fast Computing Machines," The Journal of Chemical Physics, 21(6), pp. 1087–1092.
[92] Zipay, J. J., Modlin, C. T., and Larsen, C. E., 2016, "The Ultimate Factor of Safety for Aircraft and Spacecraft - Its History, Applications and Misconceptions," *57th AIAA/ASCE/AHS/ASC Structures, Structural Dynamics, and Materials Conference*, American Institute of Aeronautics and Astronautics, San Diego, California, USA.
[93] Chandomí-Castellanos, E., Escobar-Gómez, E. N., Aguilar Marroquín-Cano, S. F., Hernandez-de-León, H. R., Velázquez-Trujillo, S., Sarmiento-Torres, J. A., and de-Coss-Pérez, C. V., 2022, "Modified Simulated Annealing Hybrid Algorithm to Solve the Traveling Salesman Problem," *2022 8th International Conference on Control, Decision and Information Technologies (CoDIT)*, pp. 1536–1541.
[94] Ford, S. L. N., 2014, "Additive Manufacturing Technology: Potential Implications for U.S. Manufacturing Competitiveness," Journal of International Commerce, Economics and Policy, 6(1), pp. 40–74.
[95] Atzeni, E., and Salmi, A., 2012, "Economics of Additive Manufacturing for End-Usable Metal Parts," International Journal of Advanced Manufacturing Technology, 62(9), pp. 1147–1155.
[96] Sigmund, O., and Maute, K., 2013, "Topology Optimization Approaches," Struct Multidisc Optim, 48(6), pp. 1031–1055.
[97] Weber, S., Montero, J., Bleckmann, M., and Paetzold, K., 2020, "Parameters on Support Structure Design for Metal Additive Manufacturing," Proceedings of the Design Society: DESIGN Conference, 1, pp. 1145–1154.
[98] Aitkenhead, A., 2013, "Mesh Voxelisation."
[99] Tuszynski, J., 2014, "In_ploy hedron."
[100] Boos, E., Ihlenfeldt, S., Milaev, N., Thielsch, J., Drossel, W.-G., Bruns, M., and Elsner, B. A. M., 2022, "Topology Optimized Unit Cells for Laser Powder Bed Fusion," Berg Huettenmaenn Monatsh, 167(7), pp. 291–299.
[101] Li, W., and Yu, Z., 2021, "Heat Exchangers for Cooling Supercritical Carbon Dioxide and Heat Transfer Enhancement: A Review and Assessment," Energy Reports, 7, pp. 4085–4105.
[102] Guo, J., 2016, "Design Analysis of Supercritical Carbon Dioxide Recuperator," Applied Energy, 164, pp. 21–27.
[103] Ziev, T., Rasouli, E., Tano, I.-N., Wu, Z., Rao Yarasi, S., Lamprinakos, N., Seo, J., Narayanan, V., Rollett, A. D., and Vaishnav, P., 2023, "Cost of Using Laser Powder Bed Fusion to Fabricate a Molten Salt-to-Supercritial Carbon Dioxide Heat Exchanger for Concentrating Solar Power," 3D Printing and Additive Manufacturing.

[104] Chen, Q., Liang, X., Hayduke, D., Liu, J., Cheng, L., Oskin, J., Whitmore, R., and To, A. C., 2019, "An Inherent Strain Based Multiscale Modeling Framework for Simulating Part-Scale Residual Deformation for Direct Metal Laser Sintering," Additive Manufacturing, 28, pp. 406–418.
[105] Bagheri, Z. S., Melancon, D., Liu, L., Johnston, R. B., and Pasini, D., 2017, "Compensation Strategy to Reduce Geometry and Mechanics Mismatches in Porous Biomaterials Built with Selective Laser Melting," Journal of the Mechanical Behavior of Biomedical Materials, 70, pp. 17–27.
[106] Pham, D. T., and Wang, X., 2000, "Prediction and Reduction of Build Times for the Selective Laser Sintering Process," Proceedings of the Institution of Mechanical Engineers, Part B: Journal of Engineering Manufacture, 214(6), pp. 425–430.
[107] Li, D., Liao, W., Dai, N., Dong, G., Tang, Y., and Xie, Y. M., 2018, "Optimal Design and Modeling of Gyroid-Based Functionally Graded Cellular Structures for Additive Manufacturing," Computer-Aided Design, 104, pp. 87–99.
[108] Gosselin, L., Tye-Gingras, M., and Mathieu-Potvin, F., 2009, "Review of Utilization of Genetic Algorithms in Heat Transfer Problems," International Journal of Heat and Mass Transfer, 52(9), pp. 2169–2188.
[109] Chang, P. S., and Rosen, D. W., 2013, "The Size Matching and Scaling Method: A Synthesis Method for the Design of Mesoscale Cellular Structures," International Journal of Computer Integrated Manufacturing, 26(10), pp. 907–927.
[110] Bugatti, M., and Semeraro, Q., 2018, "Limitations of the Inherent Strain Method in Simulating Powder Bed Fusion Processes," Additive Manufacturing, 23, pp. 329–346.
[111] Miki, T., and Yamada, T., 2021, "Topology Optimization Considering the Distortion in Additive Manufacturing," Finite Elements in Analysis and Design, 193, p. 103558.
[112] Mayer, T., Brändle, G., Schönenberger, A., and Eberlein, R., 2020, "Simulation and Validation of Residual Deformations in Additive Manufacturing of Metal Parts," Heliyon, 6(5), p. e03987.
[113] Setien, I., Chiumenti, M., van der Veen, S., San Sebastian, M., Garciandía, F., and Echeverría, A., 2019, "Empirical Methodology to Determine Inherent Strains in Additive Manufacturing," Computers & Mathematics with Applications, 78(7), pp. 2282–2295.
[114] Gruber, K., Ziółkowski, G., Pawlak, A., and Kurzynowski, T., 2022, "Effect of Stress Relief and Inherent Strain-Based Pre-Deformation on the Geometric Accuracy of Stator Vanes Additively Manufactured from Inconel 718 Using Laser Powder Bed Fusion," Precision Engineering, 76, pp. 360–376.